



©2000 IMAGE 100 LTD.

# Serpentine Locomotion with Robotic Snakes

By Masashi Saito, Masakazu Fukaya, and Tetsuya Iwasaki

**M**ost currently available mobile robot mechanisms for ground operations have wheels driven by some type of rotational motion generator such as an engine. Such wheeled mechanisms are relatively efficient, easy to steer, and suited for high-speed driving on a smooth surface. They are not effective, however, in rugged environments such as rough and/or muddy terrains. Mobile robots with

legs are being actively researched (e.g., [1]-[4]) for several reasons, including the fact that legs provide higher terrain adaptability than wheels. Even higher terrain adaptability may be achieved by multilink articulated robots that "crawl" like snakes.

Beyond their adaptability to the environment, serpentine robots offer a variety of advantages over mobile robots with wheels or legs. They are robust to mechanical failure because they are modular and highly redundant. They may

---

Iwasaki ([iwasaki@virginia.edu](mailto:iwasaki@virginia.edu)) is with the Department of Mechanical and Aerospace Engineering, University of Virginia, P.O. Box 400746, Charlottesville, VA 22904-4746, U.S.A. Saito is with the Automotive Products Division, Hitachi, Ltd., Ibaraki, Japan. Fukaya is with the Network Services Group, Outsourcing Integration Division, System Center Solution Department, Fujitsu Ltd., Tokyo, Japan.

also perform as manipulator arms when part of the multilinked body is fixed to a platform. On the other hand, one of the main drawbacks is their poor power efficiency for surface locomotion. Another is the difficulty in analyzing and synthesizing snakelike locomotion mechanisms, which are not as simple as wheeled mechanisms. While the former is a fundamental drawback inherent to snakelike locomotion, the latter point has been addressed by many researchers [5]-[15], and we hope to add another contribution to overcoming the difficulty.

In this article, we consider a snake robot *without wheels* that has substantial potential for adapting to the environment, at the expense of power efficiency. Our objective is to establish a mathematical framework for the modeling, analysis, and synthesis of serpentine locomotion with a multilink robotic snake. We apply some existing knowledge from the biological study of snakes, but our focus will be on a robotic realization theory of snakelike locomotion rather than the biomimetic aspect of the problem. We restrict our attention to planar serpentine gait of locomotion, and hence the more general three-dimensional motion and other gaits on isotropic friction environments are beyond the scope of this article.

First, we develop a mathematical model for an articulated snake robot consisting of  $n$  rigid links with torque actuators at  $n-1$  joints. Two models for the directional friction force acting on each link are developed and integrated into the total equations of motion for the snake robot. We then show a model transformation that decouples the dynamics into the internal shape motion (joint torques  $\rightarrow$  joint angles) and the inertial locomotion (joint angles  $\rightarrow$  inertial position and orientation). This decoupling enables us to concentrate on control of the inertial locomotion through the shape change, assuming that the shape can readily be controlled as desired via the joint actuators.

We then analyze the locomotion of the snake robot with serpentine gait from the power efficiency standpoint. In particular, we investigate the shape motion that achieves the locomotion at a prescribed speed while requiring the least input power. Based on the analysis results, we determine the feedback control architecture to realize the desired locomotion and propose a method for designing such controllers by suggesting a quasi-linearizing input transformation. Finally, our control strategy is experimentally validated by a five-link articulated snake robot. To our knowledge, this is the first research that addresses the problem of modeling, analysis, and feedback synthesis of serpentine locomotion by an articulated robotic snake without wheels.

We use the following notation. The sets of  $n$ -dimensional real vectors and  $n \times m$  real matrices are denoted by  $\mathbb{R}^n$  and  $\mathbb{R}^{n \times m}$ , respectively. For a matrix  $M$ , the transpose is denoted by  $M'$ . For scalars  $x_1, \dots, x_n$ ,  $\text{diag}(x_1, \dots, x_n)$  denotes the  $n \times n$  diagonal matrix with  $x_1, \dots, x_n$  on the diagonal. For vectors  $x$  and  $y$ ,  $x^2$  denotes the vector with the  $i$ th entry  $x_i^2$ , while  $x/y$  denotes the vector with the  $i$ th entry  $x_i/y_i$ . The derivative of

a signal  $x(t)$  with respect to time  $t$  is denoted by  $\dot{x}(t)$  (i.e.,  $\dot{x} := dx/dt$ ). For a scalar-valued periodic signal  $x(t)$ ,  $\text{ave}(x)$  is the average value of  $x(t)$  over a period. The signum function is denoted by  $\text{sgn}(\cdot)$ ; i.e.,  $\text{sgn}(x)$  is 1 if  $x > 0$ , 0 if  $x = 0$ , and -1 if  $x < 0$ . For a generic function  $f(x): \mathbb{R} \rightarrow \mathbb{R}$  such as  $\text{sgn}$ ,  $\sin$ , and  $\cos$ , we may let it admit a vector-valued argument with a slight abuse of notation, in which case the function operates on each entry of the argument vector. A similar comment applies to functions with two arguments, e.g.,  $\text{sat}(\cdot, \cdot)$  and  $\text{dcs}(\cdot, \cdot)$ , defined in "Some Integral Formulas" on p. 74.

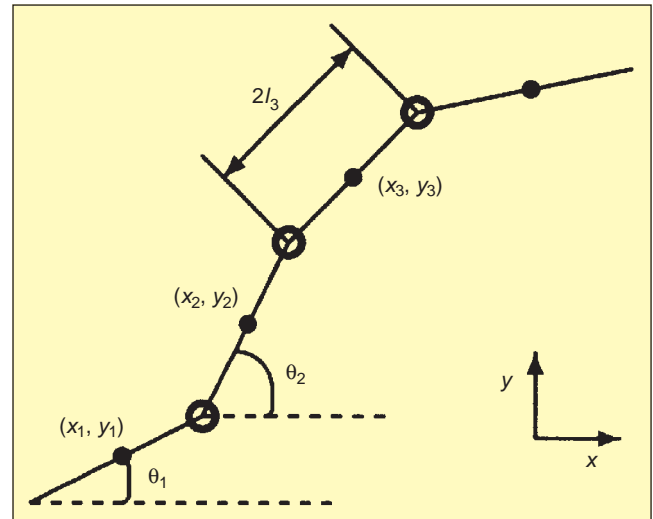


**Figure 1.** Snake robot.

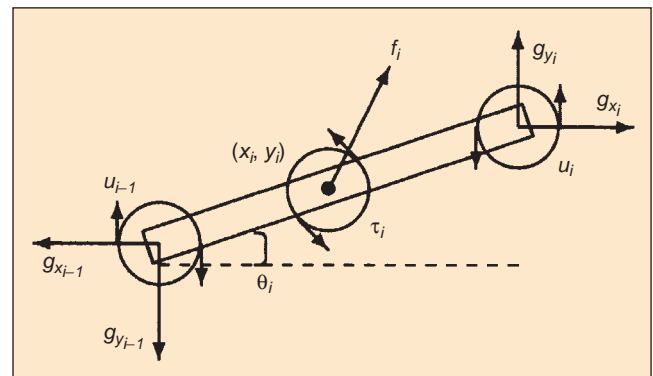


**Figure 2.** Free-body diagram for the  $i$ th link.

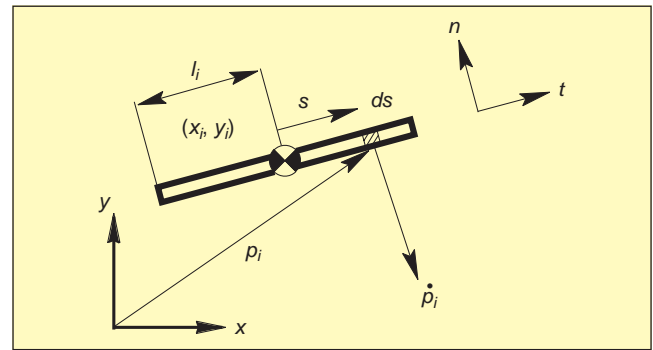


**Figure 3.** Infinitesimal segment on the  $i$ th link.

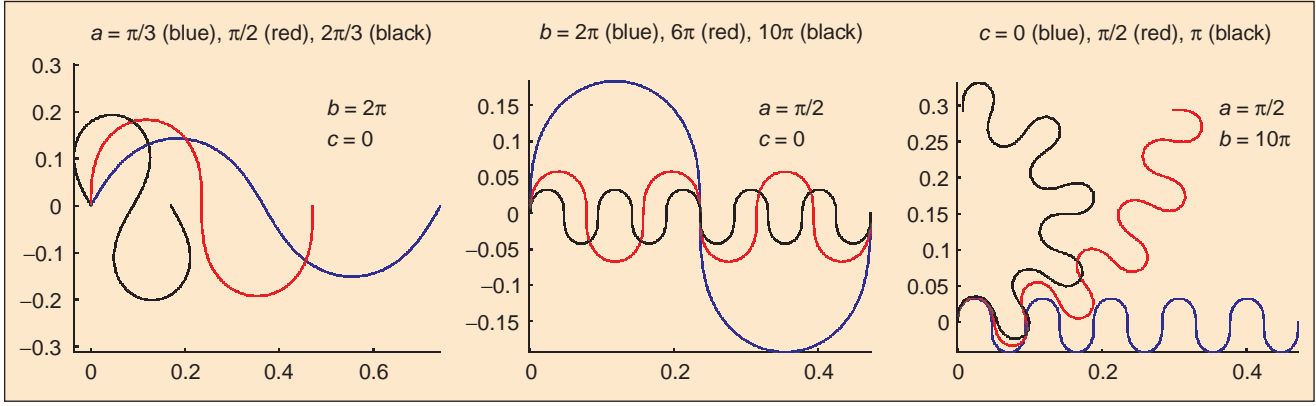


**Figure 4.** Various serpenoid curves.

## Snake Locomotion

Research in experimental biology (e.g., [16], [17]) has revealed the mechanisms of the four common modes (or gaits) of locomotion in snakes: serpentine, side-winding, concertina, and rectilinear. Further analysis of snake locomotion was also done from biological standpoints [18]-[21], as well as from mechanical perspectives [22], [23]. A successful robotic realization of serpentine locomotion was first reported in [24], and the research results are summarized in [25].

Hirose [25], [26] studied snakes and found that their bodies take on the so-called serpenoid curve when they locomote with a serpentine gait. Moreover, the key property of snakes in achieving serpentine locomotion is the difference in the friction coefficients for the tangential and the normal directions with respect to the body. In particular, the normal friction tends to be much larger than the tangential friction, leading to avoidance of side slipping. Based on this fact, Hirose built snakelike locomotors and developed a control method to make them move in a desired direction at a desired speed. The locomotors had wheels to realize the

directional friction and the control was open loop in nature, and hence adaptability to the environment was somewhat weakened. Nevertheless, the control scheme was very intuitive and constituted a solid foundation for the study of robotic serpentine locomotion.

Another notable result in snakelike robotic mechanisms has been obtained by Burdick et al. [27]-[29]. They studied, with mathematical rigor and experimental validation, the mechanism of “undulatory locomotion” in which net motion is generated by the coupling between internal shape changes and external nonholonomic constraints. The problem considered is kinematic rather than dynamic in nature due to the nonholonomic constraints arising from idealization of wheels such that they do not slip in the direction of the rotational axis. Other results on serpentine locomotion in the nonholonomic setting include those described in [30]-[32]. Again, an essential assumption in these results is that serpentine robots have wheels, and thus the main advantage of serpentine locomotion, adaptability to the environment, cannot be fully realized.

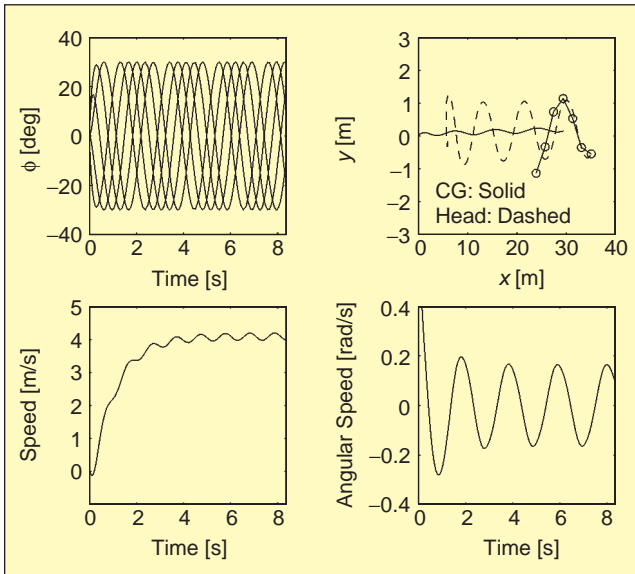


**Figure 5.** Serpentine locomotion ( $\gamma = 0^\circ$ ).

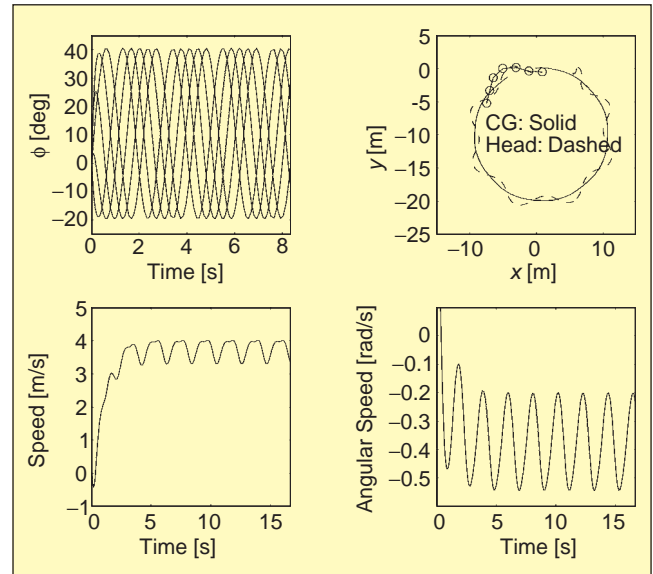


**Figure 6.** Serpentine locomotion ( $\gamma = 10^\circ$ ).

## Modeling of a Snake Robot

Consider the snake robot depicted in Fig. 1, which consists of  $n$  links connected through  $n-1$  joints. Each link is rigid with uniformly distributed mass. Each joint is equipped with a torque actuator (motor). The snake robot is placed on a horizontal surface, and we consider only planar motion; in this case, the mechanical system has  $n+2$  degrees of freedom ( $n-1$  for shape, 2 for position, and 1 for orientation).

Later, we will develop dynamic equations of motion for the snake robot. To this end, let us introduce some notation. Fix  $x - y$  axes in the inertial frame and consider the  $i$ th link of the snake robot. The link is of mass  $m_i$ , length  $2l_i$ , and moment of inertia  $J_i (= m_i l_i^2 / 3)$ . Let  $(x_i, y_i)$  and  $\theta_i$  be the coordinates of the center of gravity and the angle between the link and the  $x$ -axis, respectively. Denote by  $x$ ,  $y$ , and  $\theta$  the  $n$ -dimensional vectors whose  $i$ th entries are  $x_i$ ,  $y_i$ , and  $\theta_i$ , respectively. Define

$$A := \begin{bmatrix} 1 & 1 & & \\ & \ddots & \ddots & \\ & & 1 & 1 \end{bmatrix} \in \mathbb{R}^{(n-1) \times n}$$

$$D := \begin{bmatrix} 1 & -1 & & \\ & \ddots & \ddots & \\ & & 1 & -1 \end{bmatrix} \in \mathbb{R}^{(n-1) \times n}$$

$$E := \begin{bmatrix} e & 0 \\ 0 & e \end{bmatrix}, \quad e := [1 \dots 1]' \in \mathbb{R}^n, \quad m := \sum_{i=1}^n m_i$$

$$S_\theta := \text{diag}(\sin \theta_1, \dots, \sin \theta_n), \quad C_\theta := \text{diag}(\cos \theta_1, \dots, \cos \theta_n),$$

$$J := \text{diag}(J_1, \dots, J_n), \quad M := \text{diag}(m_1, \dots, m_n),$$

$$L := \text{diag}(l_1, \dots, l_n), \quad H := LA' (DM^{-1}D')^{-1} AL,$$

$$N := M^{-1}D' (DM^{-1}D')^{-1} AL, \quad \mathcal{J} := J + S_\theta HS_\theta + C_\theta HC_\theta,$$

$$\mathcal{C} := S_\theta HC_\theta - C_\theta HS_\theta, \quad \mathcal{L} := [S_\theta N' \quad -C_\theta N']'$$

$$\mathcal{B} := D\mathcal{J}^{-1}D', \quad \mathcal{K} := \mathcal{J}^{-1}D'\mathcal{B}^{-1}, \quad \rho := 1/(e' \mathcal{J} e), \quad e_\rho := \rho e.$$

In the above, the symbols  $D$  and  $A$  stand for the “difference” and the “addition” operators, respectively. The vector  $e$  is a basis of the kernel of  $D$ . It can be shown that the matrices  $\mathcal{J}$  and  $\mathcal{C}$  depend on the relative angles  $\phi := D\theta$  only, and thus are determined by the shape of the snake robot.

Consider the free-body diagram for the  $i$ th link depicted in Fig. 2, where  $f_i$  and  $\tau_i$  are the force and the torque due to the friction between the link and the horizontal surface,  $g_i$  and  $g_{i-1}$  are the constraint forces from the adjacent links, and  $u_i$  and  $u_{i-1}$  are the joint torques from the actuators. Let  $\tau \in \mathbb{R}^n$  be the vector whose  $i$ th entry is  $\tau_i$ , and similarly for  $f_x, f_y \in \mathbb{R}^n$  and  $g_x, g_y, u \in \mathbb{R}^{n-1}$ , where  $(f_x, f_y)$  and  $(g_x, g_y)$  are the

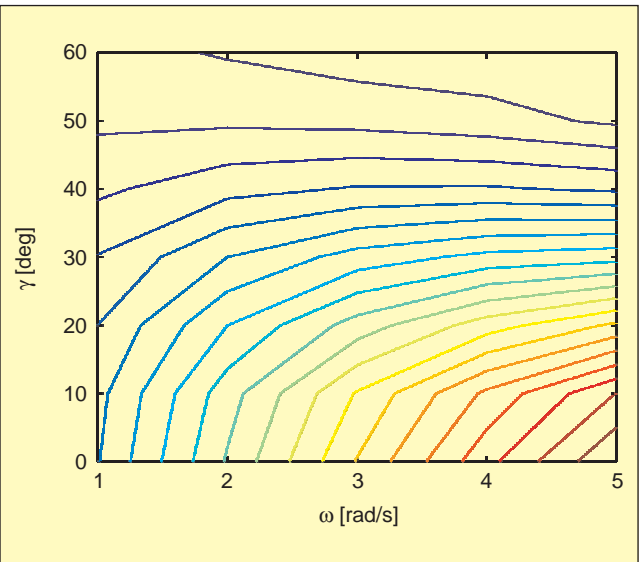


**Figure 7.** Contour plot of the average speed as a function of  $\omega$  and  $\gamma$ .

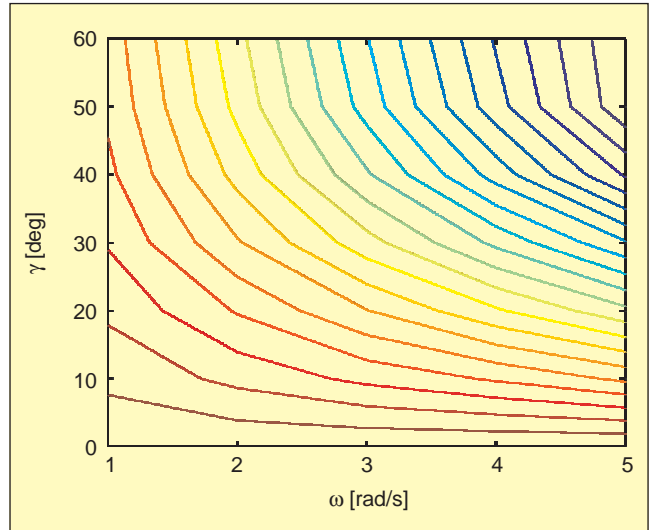


**Figure 8.** Contour plot of the average angular speed as a function of  $\omega$  and  $\gamma$ .

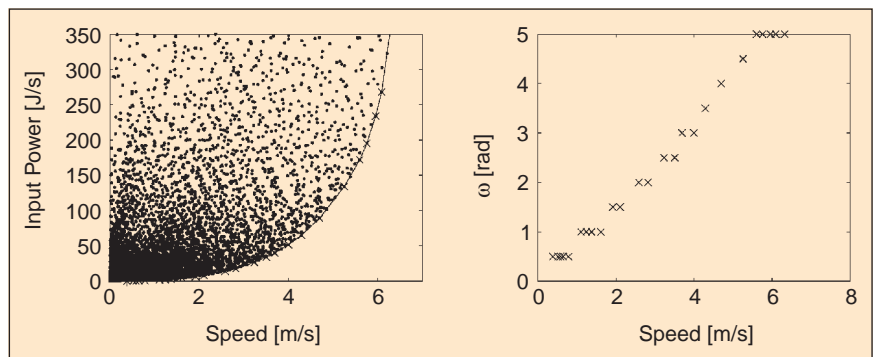


**Figure 9.** Speed/power trade-off.

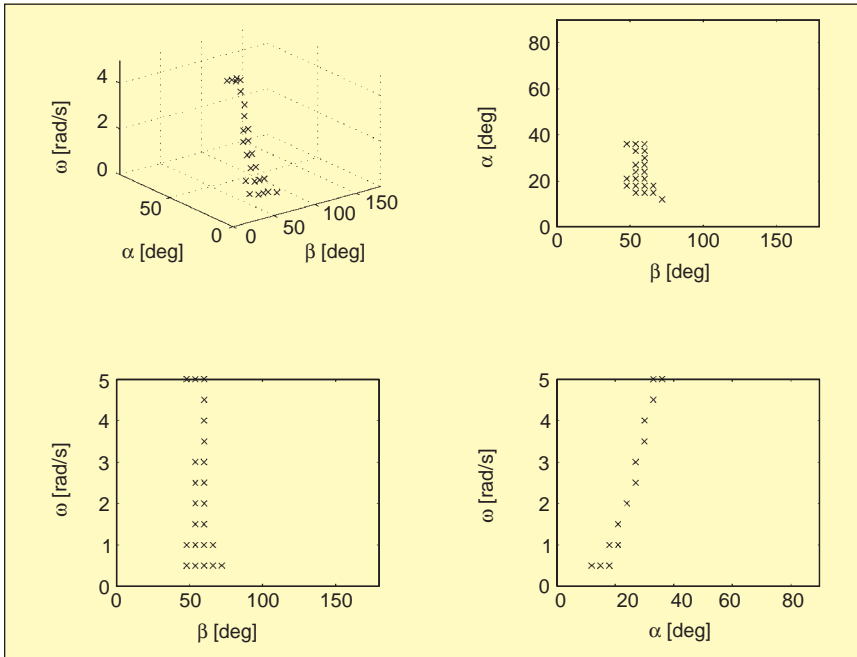


**Figure 10.** Pareto-optimal parameters.

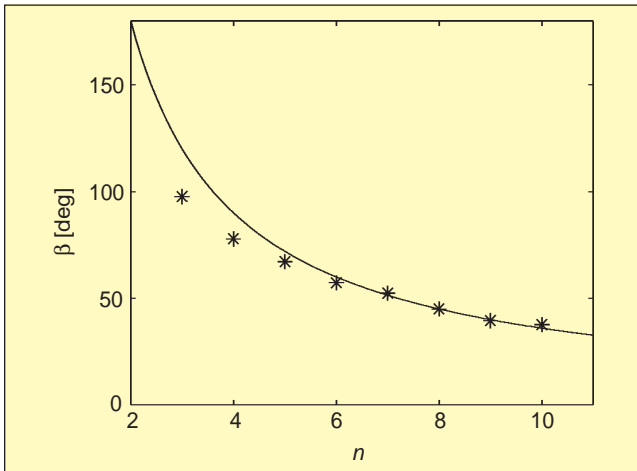


**Figure 11.** Phase shift  $\beta$  versus the number of links  $n$ .

$(x, y)$  components of the friction force vector  $f_i$  and the constraint force vector  $g_i$ , respectively. Finally, we define the total friction force vector  $f$  and the whole position vector  $z$  by

$$f := \begin{bmatrix} f_x \\ f_y \end{bmatrix}, \quad z := \begin{bmatrix} x \\ y \end{bmatrix}.$$

We shall first develop two friction models based on a simplified viscous friction and a Coulomb friction to give expressions for  $f$  and  $\tau$  in terms of  $x$ ,  $y$ , and  $\theta$ . Equations of motion will then be derived using the friction models.

### Simple Friction Model

Consider the  $i$ th link of the snake robot depicted in Fig. 3. The coordinates of the infinitesimal segment  $ds$  are given by

$$p_i = \begin{bmatrix} x_i \\ y_i \end{bmatrix} + \begin{bmatrix} \cos\theta_i & \sin\theta_i \\ \sin\theta_i & -\cos\theta_i \end{bmatrix} s.$$

Taking the derivative with respect to time, we have the velocity vector in the  $x$ - $y$  frame

$$\dot{p}_i = \begin{bmatrix} \dot{x}_i \\ \dot{y}_i \end{bmatrix} + \begin{bmatrix} -\sin\theta_i & \cos\theta_i \\ \cos\theta_i & \sin\theta_i \end{bmatrix} s\dot{\theta}_i.$$

The tangential and normal components of the velocity vector  $\dot{p}_i$  are given by

$$\begin{aligned} \begin{bmatrix} \tilde{v}_{t_i} \\ \tilde{v}_{n_i} \end{bmatrix} &:= \begin{bmatrix} \cos\theta_i & \sin\theta_i \\ -\sin\theta_i & \cos\theta_i \end{bmatrix} \begin{bmatrix} \dot{x}_i \\ \dot{y}_i \end{bmatrix} \\ \dot{p}_i &= \begin{bmatrix} v_{t_i} \\ v_{n_i} \end{bmatrix} + \begin{bmatrix} 0 \\ s\dot{\theta}_i \end{bmatrix} \end{aligned} \quad (1)$$

where

$$\begin{bmatrix} v_{t_i} \\ v_{n_i} \end{bmatrix} := \begin{bmatrix} \cos\theta_i & \sin\theta_i \\ -\sin\theta_i & \cos\theta_i \end{bmatrix} \begin{bmatrix} \dot{x}_i \\ \dot{y}_i \end{bmatrix}. \quad (2)$$

Now assume that the friction force is modeled in the body ( $t$ - $n$ ) frame as

$$\begin{bmatrix} df_{t_i} \\ df_{n_i} \end{bmatrix} = -\begin{bmatrix} c_{t_i} & 0 \\ 0 & c_{n_i} \end{bmatrix} \begin{bmatrix} \tilde{v}_{t_i} \\ \tilde{v}_{n_i} \end{bmatrix} dm_i$$

where  $c_{t_i}$  and  $c_{n_i}$  are the friction coefficients and  $dm_i$  is the mass of the infinitesimal segment [i.e.,  $dm_i = (m_i ds) / (2l_i)$ ]. Transforming the coordinates, the friction force in the inertial frame is

$$\begin{bmatrix} df_{x_i} \\ df_{y_i} \end{bmatrix} = \begin{bmatrix} \cos\theta_i & -\sin\theta_i \\ \sin\theta_i & \cos\theta_i \end{bmatrix} \begin{bmatrix} df_{t_i} \\ df_{n_i} \end{bmatrix}.$$

Integrating over the link, the total friction force is given by

$$\begin{bmatrix} f_{x_i} \\ f_{y_i} \end{bmatrix} = -m_i \begin{bmatrix} \cos\theta_i & -\sin\theta_i \\ \sin\theta_i & \cos\theta_i \end{bmatrix} \begin{bmatrix} c_{t_i} & 0 \\ 0 & c_{n_i} \end{bmatrix} \begin{bmatrix} \cos\theta_i & \sin\theta_i \\ -\sin\theta_i & \cos\theta_i \end{bmatrix} \begin{bmatrix} \dot{x}_i \\ \dot{y}_i \end{bmatrix}.$$

Finally, the total friction torque around the center of mass of the link is

$$\tau_i = \int s \, df_{n_i} = -\frac{m_i l_i^2}{3} c_{n_i} \dot{\theta}_i = -c_{n_i} J_i \dot{\theta}_i$$

where the positive direction is counterclockwise.

We now consider the whole system of connected links. It can be verified that the total friction force and torque acting on the system can be expressed as

$$\begin{aligned} f &= -\Omega_\theta D_r \Omega'_\theta \dot{z} \\ \tau &= -D_\tau \dot{\theta} \end{aligned} \quad (3)$$

where

$$\begin{aligned} D_r &:= \begin{bmatrix} C_r M & 0 \\ 0 & C_n M \end{bmatrix}, \quad D_\tau := C_n J, \quad \Omega_\theta := \begin{bmatrix} C_\theta & -S_\theta \\ S_\theta & C_\theta \end{bmatrix}, \\ C_r &:= \text{diag}(c_{t_1}, \dots, c_{t_n}), \quad C_n := \text{diag}(c_{n_1}, \dots, c_{n_n}). \end{aligned} \quad (4)$$

### Coulomb Friction Model

As in the previous section, we give the expression for the tangential and normal velocity components (1). Assume that the friction force acting on the infinitesimal segment is given by

$$\begin{bmatrix} df_{t_i} \\ df_{n_i} \end{bmatrix} = -g \begin{bmatrix} \mu_{t_i} & 0 \\ 0 & \mu_{n_i} \end{bmatrix} \begin{bmatrix} \text{sgn}(\tilde{v}_{t_i}) \\ \text{sgn}(\tilde{v}_{n_i}) \end{bmatrix} dm_i,$$

where  $\mu_{t_i}$  and  $\mu_{n_i}$  are, respectively, the Coulomb friction coefficients in the tangential and the normal directions,  $g$  is the gravity constant, and  $dm_i$  is the mass of the segment. Integrating over the link, the total friction force acting on the  $i$ th link is

$$\begin{bmatrix} f_{t_i} \\ f_{n_i} \end{bmatrix} = -g \begin{bmatrix} \mu_{t_i} & 0 \\ 0 & \mu_{n_i} \end{bmatrix} \int_{-l_i}^{l_i} \frac{m_i}{2l_i} \begin{bmatrix} \text{sgn}(\tilde{v}_{t_i}) \\ \text{sgn}(\tilde{v}_{n_i}) \end{bmatrix} ds.$$

Similarly, the total torque is given by

$$\tau_i = \int s df_{n_i} = -\frac{\mu_{n_i} m_i g}{2l_i} \int_{-l_i}^{l_i} \text{sgn}(\tilde{v}_{n_i}) s ds.$$

Using Lemma 1 (see “Some Integral Formulas”), we have

$$\begin{aligned} \begin{bmatrix} f_{x_i} \\ f_{y_i} \end{bmatrix} &= -m_i g \begin{bmatrix} \cos\theta_i & -\sin\theta_i \\ \sin\theta_i & \cos\theta_i \end{bmatrix} \begin{bmatrix} \mu_{t_i} & 0 \\ 0 & \mu_{n_i} \end{bmatrix} \text{sat}\left(\begin{bmatrix} v_{t_i} \\ v_{n_i} \end{bmatrix}, \begin{bmatrix} 0 \\ l_i \dot{\theta}_i \end{bmatrix}\right) \\ \tau_i &= -\frac{1}{2} \mu_{n_i} m_i g l_i \int dz \text{ds}(\tilde{v}_{n_i}, l_i \dot{\theta}_i). \end{aligned}$$

Assembling the above expressions into vector form, the total friction force and torque can be given by

$$\begin{aligned} f &= -\Omega_\theta \Delta_r \text{sat}(\Omega'_\theta \dot{z}, \Lambda \dot{\theta}) \\ \tau &= -\Delta_\tau \int dz \text{ds}(\Gamma_\theta \dot{z}, L \dot{\theta}) \end{aligned} \quad (5)$$

where

$$\begin{aligned} \Delta_r &:= \begin{bmatrix} \mu_r Mg & 0 \\ 0 & \mu_n Mg \end{bmatrix}, \quad \Lambda := \begin{bmatrix} 0 \\ L \end{bmatrix}, \\ \Delta_\tau &= \frac{1}{2} \mu_n Mg L, \quad \Gamma_\theta := \begin{bmatrix} -S_\theta & C_\theta \end{bmatrix} \\ \mu_r &:= \text{diag}(\mu_{t_1}, \dots, \mu_{t_n}), \quad \mu_n := \text{diag}(\mu_{n_1}, \dots, \mu_{n_n}). \end{aligned}$$

### Equations of Motion

Applying first principles to the free-body diagram of the  $i$ th link in Fig. 2 and assembling into the  $n$ -link snake robot, we obtain the equations of translational motion

$$\begin{aligned} M\ddot{x} &= f_x + D' g_x \\ M\ddot{y} &= f_y + D' g_y \end{aligned} \quad (6)$$

and the equation of rotational motion

$$J\ddot{\theta} = \tau - S_\theta L A' g_x + C_\theta L A' g_y + D' u. \quad (7)$$

Recall that the snake robot has  $n+2$  degrees of freedom, and we have used  $3n$  variables ( $x$ ,  $y$ , and  $\theta$ ) to describe its motion. Below, we will develop equations of motion in terms of the absolute angles  $\theta$  and the position of the center of gravity

$$w := \begin{bmatrix} w_x \\ w_y \end{bmatrix} = \frac{1}{m} \begin{bmatrix} e' M x \\ e' M y \end{bmatrix}.$$

In view of Fig. 1, the vectors  $x$ ,  $y$ , and  $\theta$  are constrained by

$$\begin{aligned} Dx + AL \cos\theta &= 0 \\ Dy + AL \sin\theta &= 0. \end{aligned} \quad (8)$$

From the definition of  $w$  and (8), we have

$$Tx = \begin{bmatrix} -AL \cos\theta \\ w_x \end{bmatrix}, \quad Ty = \begin{bmatrix} -AL \sin\theta \\ w_y \end{bmatrix}, \quad T := \begin{bmatrix} D \\ e' M/m \end{bmatrix}.$$

Solving these equations for  $x$  and  $y$  and taking the time derivatives, we see that the translational velocity is given by

$$\dot{z} = \mathcal{L}\dot{\theta} + E\dot{w} \quad (9)$$

where we noted that

$$T^{-1} = \begin{bmatrix} M^{-1} D' (DM^{-1} D')^{-1} & e \end{bmatrix}.$$

Next we decompose the equations of translational motion (6) into two parts: expressions for the center of mass acceleration  $\ddot{w}$  and the constraint forces  $g_x$  and  $g_y$ . Multiplying (6) by  $T M^{-1}$  from the left, we have

$$T\ddot{x} = \begin{bmatrix} D\ddot{x} \\ \ddot{w}_x \end{bmatrix} = \begin{bmatrix} DM^{-1} f_x + DM^{-1} D' g_x \\ e' f_x / m \end{bmatrix} \quad (10)$$

for the  $x$  coordinate and similarly for the  $y$  coordinate. Solving for  $g_x$  and  $g_y$ , we have

$$\begin{aligned} g_x &= (DM^{-1} D')^{-1} (AL(C_\theta \dot{\theta}^2 + S_\theta \ddot{\theta}) - DM^{-1} f_x) \\ g_y &= (DM^{-1} D')^{-1} (AL(S_\theta \dot{\theta}^2 - C_\theta \ddot{\theta}) - DM^{-1} f_y) \end{aligned} \quad (11)$$

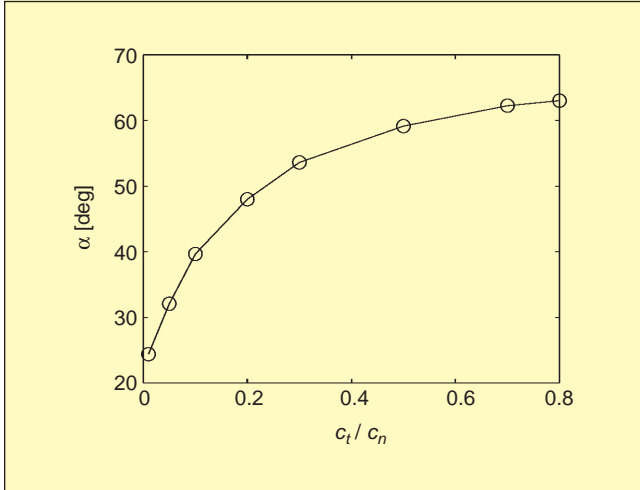


**Figure 12.** Undulation angle  $\alpha$  versus the ratio of friction coefficients  $c_t / c_n$ .

where we noted from (8) that

$$D\ddot{x} = AL(C_\theta \dot{\theta}^2 + S_\theta \ddot{\theta}), \quad D\ddot{y} = AL(S_\theta \dot{\theta}^2 - C_\theta \ddot{\theta}).$$

Substituting (11) into (7) and using the second row of (10), we have

$$\begin{aligned} \ddot{\theta} + C\dot{\theta}^2 &= D'u + \tau + L'f \\ m\ddot{w} &= E'f. \end{aligned} \quad (12) \quad \text{where}$$

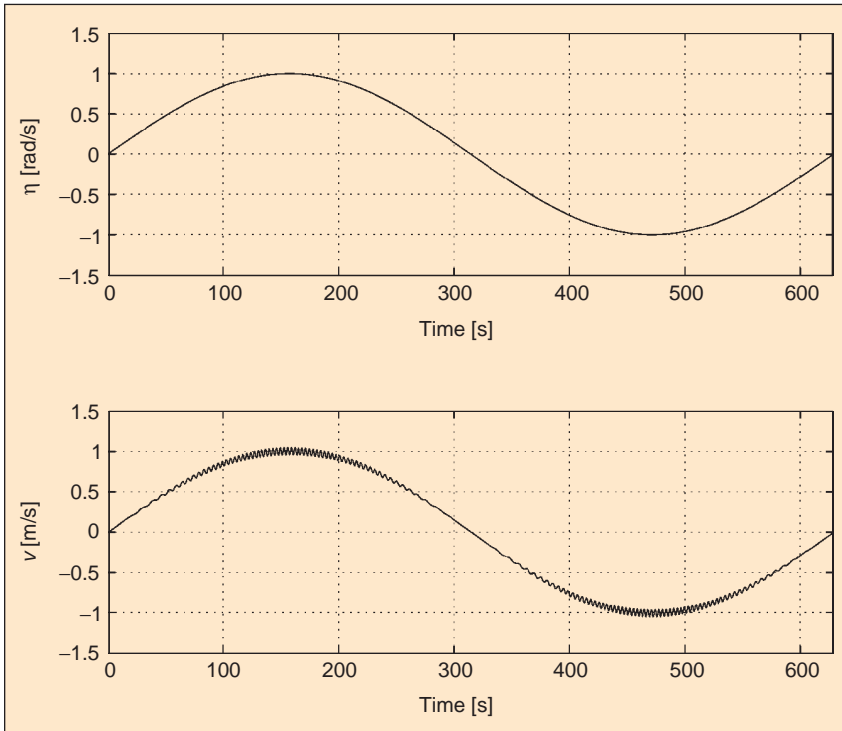


**Figure 14.** Speed response  $v$  for sinusoidal input  $\dot{\eta}$  with  $\lambda = 0.01$ .

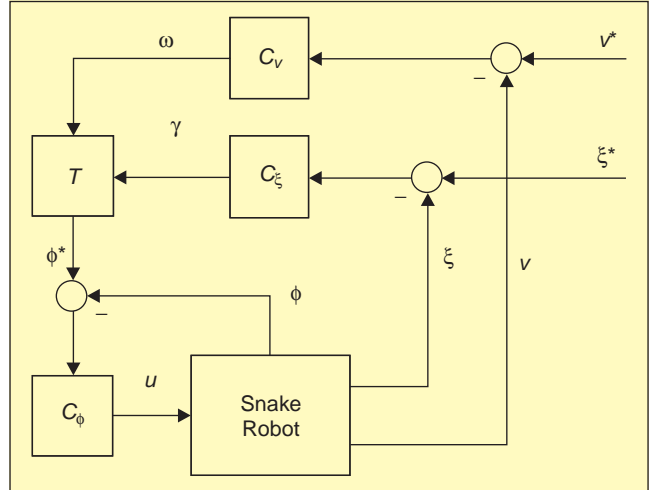


**Figure 13.** Control system configuration.

The complete set of equations of motion is now derived: (12), (9), and (3) for the simple friction model and (5) for the Coulomb friction model. In the former case, all these equations can be assembled into the following:

$$\begin{bmatrix} \mathcal{J} & 0 \\ 0 & mI \end{bmatrix} \begin{bmatrix} \dot{\theta} \\ \ddot{w} \end{bmatrix} + \begin{bmatrix} C\dot{\theta}^2 \\ 0 \end{bmatrix} + \begin{bmatrix} \mathcal{R} & \mathcal{S} \\ \mathcal{S}' & \mathcal{Q} \end{bmatrix} \begin{bmatrix} \dot{\theta} \\ \ddot{w} \end{bmatrix} = \begin{bmatrix} D' \\ 0 \end{bmatrix} u \quad (13)$$

$$\begin{bmatrix} \mathcal{R} & \mathcal{S} \\ \mathcal{S}' & \mathcal{Q} \end{bmatrix} := \begin{bmatrix} D_\tau & 0 \\ 0 & 0 \end{bmatrix} + \begin{bmatrix} \mathcal{L}' \\ E' \end{bmatrix} \Omega_\theta D_f \Omega'_\theta \begin{bmatrix} \mathcal{L} & E \end{bmatrix} \quad (14)$$

and  $D_\tau$  and  $D_f$  are defined by (4).

### Dynamic Decoupling

In this section, we show that the dynamic equation developed in the previous section can be decoupled into two parts: the shape motion (joint torques  $\rightarrow$  joint angles) and the inertial locomotion (joint angles  $\rightarrow$  inertial position and orientation). This decoupling simplifies the analysis and synthesis of snakelike locomotion in the subsequent sections.

To this end, we first observe some properties of the snake robot dynamics. It can readily be verified that the system matrices have the following internal structures:

$$\begin{aligned} \mathcal{C} + \mathcal{C}' &= 0 \\ \mathcal{J} &= \mathcal{C}\dot{\theta} - \dot{\theta}\mathcal{C}. \end{aligned} \quad (15)$$

These properties have been found for robotic manipulators and used for control design (e.g., [33]), and will also be useful for our development below.

Define new variables as follows:

$$\begin{bmatrix} \dot{\phi} \\ \dot{\psi} \end{bmatrix} := \begin{bmatrix} D \\ e' \mathcal{J} \end{bmatrix} \dot{\theta}.$$

Note that  $\dot{\phi}$  is the vector of relative angles between adjacent bodies and  $\dot{\psi}$  can be thought of as an average angular momentum. Solving this defining equation for  $\dot{\theta}$ ,

$$\dot{\theta} = \mathcal{K} \dot{\phi} + e_p \dot{\psi}. \quad (16)$$

In view of (15), we have

$$\begin{aligned} \begin{bmatrix} \ddot{\phi} \\ \ddot{\psi} \end{bmatrix} &= \begin{bmatrix} D \ddot{\theta} \\ e' \frac{d}{dt} (\mathcal{J} \dot{\theta}) \end{bmatrix} \\ &= \begin{bmatrix} D \ddot{\theta} \\ e' (\mathcal{J} \ddot{\theta} + \mathcal{C} \dot{\theta}^2 - \dot{\theta} \mathcal{C} \dot{\theta}) \end{bmatrix} \\ &= \begin{bmatrix} D \ddot{\theta} \\ e' (\mathcal{J} \ddot{\theta} + \mathcal{C} \dot{\theta}^2) \end{bmatrix}, \end{aligned}$$

where we noted that

$$e' \dot{\theta} \mathcal{C} \dot{\theta} = \dot{\theta}' \mathcal{C} \dot{\theta} = 0$$

because  $\mathcal{C}$  is skew symmetric. Using these relationships, the original equation of motion (12) can be transformed as

$$\begin{bmatrix} D \mathcal{J}^{-1} \\ e' \end{bmatrix} (\mathcal{J} \ddot{\theta} + \mathcal{C} \dot{\theta}^2 - \tau - \mathcal{L}' f - D' u) = 0$$

or equivalently as

$$\begin{aligned} \ddot{\phi} + D \mathcal{J}^{-1} (\mathcal{C} \dot{\theta}^2 - \tau - \mathcal{L}' f) &= Bu \\ \ddot{\psi} &= e' (\tau + \mathcal{L}' f) \end{aligned} \quad (17)$$

where we used  $e' D' = 0$ .

We now see that the torque input  $u$  drives the shape  $\phi$  of the snake robot through the first equation in (17), and that the shape change  $\phi$ , when coupled with the inertial motion, generates the friction force and torque by (3) or (5) with (9) and (16). The friction force and torque thus generated drive the snake robot with respect to the inertial frame through the second equation in each of (12) and (17). In the case of the simple fric-

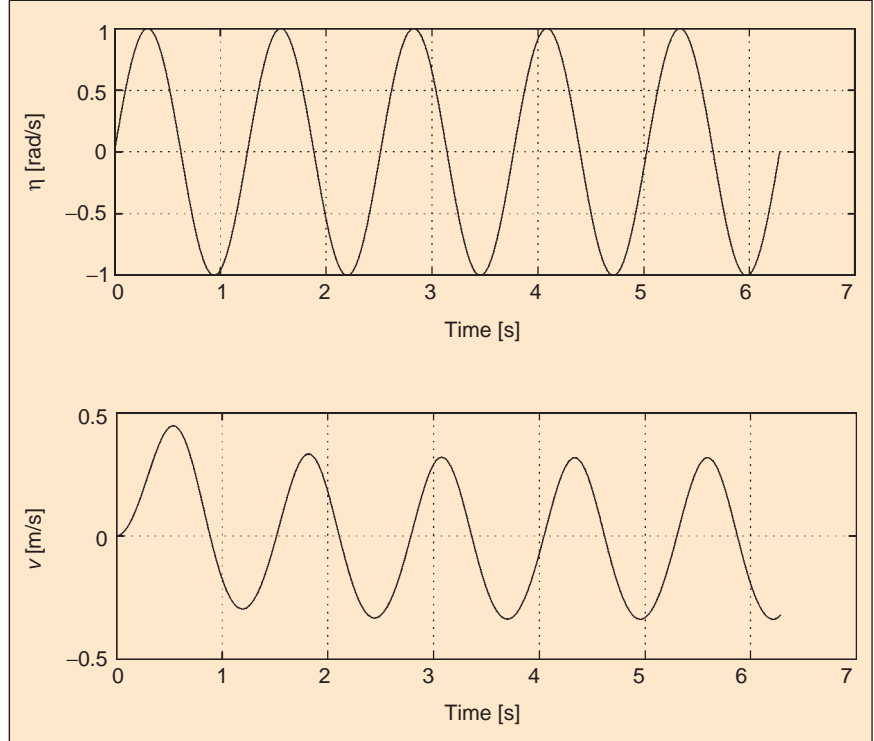


**Figure 15.** Speed response  $v$  for sinusoidal input  $\dot{\eta}$  with  $\lambda = 5$ .

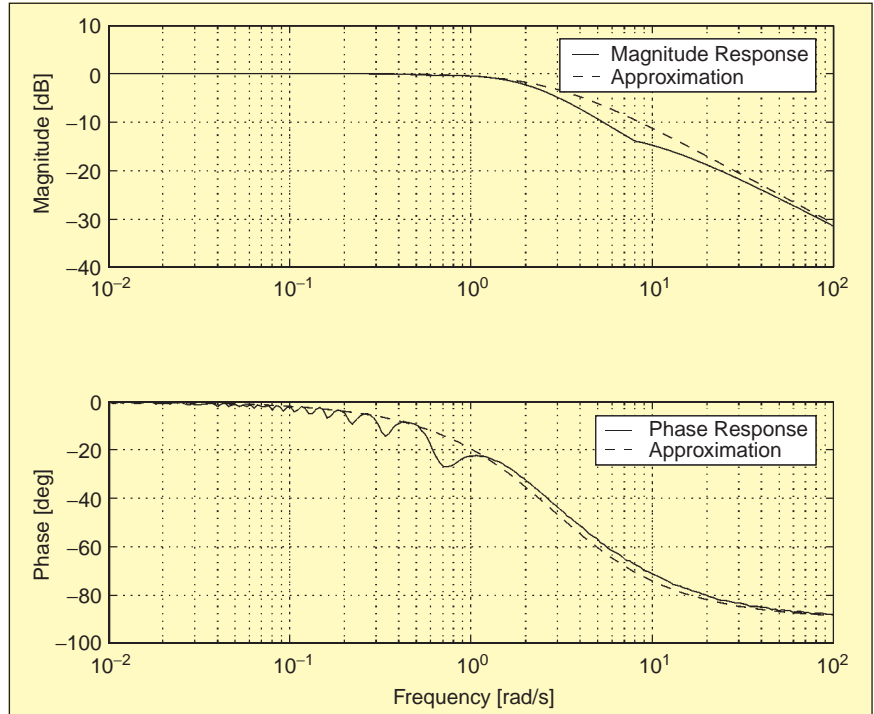


**Figure 16.** Frequency response:  $\dot{\eta} \rightarrow v$  ( $\gamma = 0$ ).

tion model (3), the rationale behind this observation may be more transparent, for the decoupled equations of motion can be concisely expressed as follows:

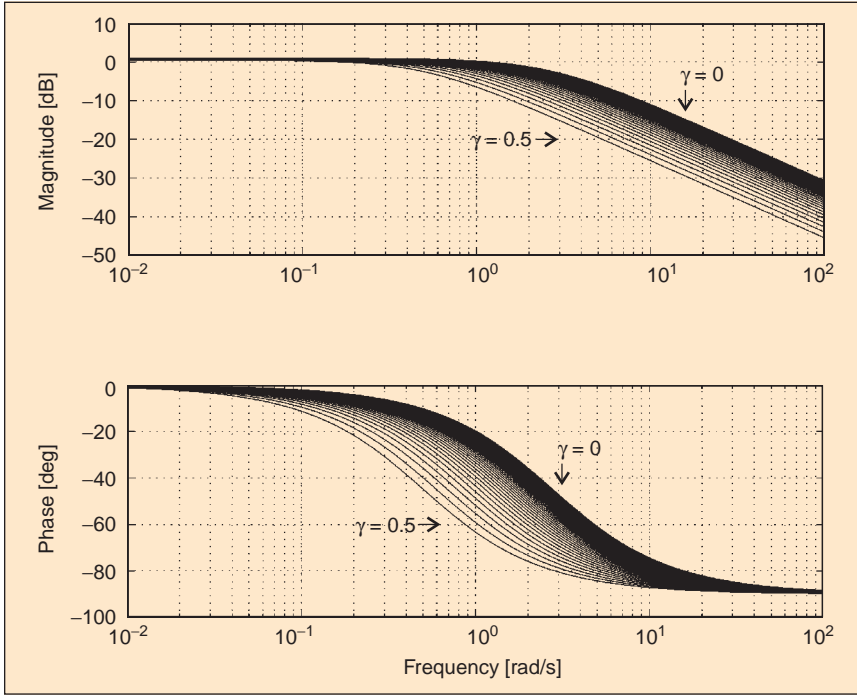


**Figure 17.** Approximated frequency responses:  $\dot{\eta} \rightarrow v (0 \leq \gamma \leq 0.5)$ .

$$\begin{bmatrix} p & 0 \\ 0 & mI \end{bmatrix} \begin{bmatrix} \ddot{\psi} \\ \ddot{w} \end{bmatrix} + \begin{bmatrix} e'_p \mathcal{R} & e'_p \mathcal{S} \\ S' e_p & Q \end{bmatrix} \begin{bmatrix} \dot{\psi} \\ \dot{w} \end{bmatrix} + \begin{bmatrix} e'_p R \\ S' \end{bmatrix} \mathcal{K} \dot{\phi} = 0 \\ \ddot{\phi} + D \mathcal{J}^{-1} (\mathcal{C} \dot{\theta}^2 + \mathcal{R} \dot{\theta} + S w) = Bu \quad (18)$$

where  $\dot{\theta}$  is given by (16).

With the decoupled equations of motion, it is natural to develop a control strategy such that:

- 1) The joint torque  $u$  controls the shape  $\phi$  of the snake robot.
- 2) The shape  $\phi$  controls the inertial behavior  $\psi$  and  $w$  of the snake robot.

Since the matrix  $B$  is nonsingular, the control in step 1 is easy. In the next section, we examine the dynamic behavior of the snake robot related to step 2 of the above control strategy. The analysis results from the next section will be useful for designing control systems to achieve snakelike locomotion in a later section.

## Analysis of Snakelike Locomotion

When the shape  $\phi$  of the snake robot changes, the force  $f$  and the torque  $\tau$  are generated due to the friction between the robot and the surface on which it lies. As a result, the position of the center of gravity  $w$  and the angular momentum of the whole body  $\psi$  change. The first equation in (18) shows how the change in  $\phi$  affects the motion variables  $\psi$  and  $w$ . If we control the shape  $\phi$  appropriately, then the snake robot will achieve the desired locomotion. Our objective in this section is to find out how to change  $\phi$  to achieve the desired

locomotion specified by speed, direction, and power efficiency.

There are at least two approaches to determining appropriate  $\phi$ : one is to optimize  $\phi$  with respect to a well-defined criterion subject to the dynamic constraint given by the first equation in (18); the other is to simply mimic the motion of living snakes. The former would be a very challenging approach, whereas the latter does not guarantee yielding a motion that is optimal for the robotic snake. Here we take an approach that fits between the two.

We will restrict our discussion to the biologically inspired serpentine locomotion [25] (i.e., the motion induced by changing the shape of the snake robot so as to form the serpenoid curves observed in living snakes). The set of serpenoid curves is characterized by several parameters. We will examine how each parameter affects the locomotion of our snake robot using the equation of motion developed earlier.

Below, we present our analysis results for the case of the simple friction model only. We also performed the same analysis using the Coulomb friction model (5) and found that the general tendency of the results is the same as the simple friction case. The analysis results will be useful for determining the appropriate shape change  $\phi$  to achieve locomotion in the desired direction, at the desired speed, with the optimal power efficiency.

## Serpenoid Curve

Let us first briefly review the serpenoid curve. It is defined [25] as follows.

**Definition 1:** Consider a curve on the  $x$ - $y$  plane that passes through the origin. It is called a *serpenoid curve* if an arbitrary point  $(x, y)$  on the curve can be expressed as

$$x(s) = \int_0^s \cos(\xi_\sigma) d\sigma, \quad y(s) = \int_0^s \sin(\xi_\sigma) d\sigma, \\ \xi_\sigma := a \cos(b \sigma) + c \sigma$$

for some scalars  $a$ ,  $b$ , and  $c$ , where  $s$  is the arc length from the origin to the point.

Fig. 4 shows several serpenoid curves of unit length generated by different choices of the parameters  $a$ ,  $b$ , and  $c$ . We see that each curve has a sinusoidlike periodic shape. The parameter  $a$  determines the degree of undulation,  $b$  determines the number of periods in a unit length, and  $c$  the macroscopic circular shape.

As has been shown in [25], the curvature of a serpenoid curve is a sinusoidal function of the arc length. In particular, it can readily be verified that

$$\kappa(s) := \sqrt{\left(\frac{d^2x}{ds^2}\right)^2 + \left(\frac{d^2y}{ds^2}\right)^2} = |a \sin(bs) - c|.$$

The curvature is related to the muscular force required for a snake to take on a given shape, and this suggests that the serpenoid curve can be considered a natural shape that a living snake takes on. See [25] for a thorough discussion with experimental justification of this statement.

Now we will give an approximation of the serpenoid curve in terms of successively connected  $n$  segments, each of which is a straight line with length  $1/n$ . Let a serpenoid curve be described by  $x(s)$  and  $y(s)$  with  $0 \leq s \leq 1$ . We consider  $n+1$  points on the curve specified by  $s_i := i/n$  ( $i = 0, \dots, n$ ). By definition, the values of  $x(s_i)$  and  $y(s_i)$  can be approximated by

$$x_i = \sum_{k=1}^i \frac{1}{n} \cos\left(a \cos\left(\frac{kb}{n}\right) + \frac{kc}{n}\right),$$

$$y_i = \sum_{k=1}^i \frac{1}{n} \sin\left(a \cos\left(\frac{kb}{n}\right) + \frac{kc}{n}\right).$$

The original serpenoid curve is then approximated by  $n$  segments connecting  $(x_i, y_i)$  ( $i = 0, \dots, n$ ).

Denote by  $\theta_i$  the angle of the  $i$ th segment measured from the  $x$ -axis in a counterclockwise manner. Then

$$\tan(\theta_i) = \frac{y_i - y_{i-1}}{x_i - x_{i-1}} = \frac{\sin(a \cos(ib/n) + ic/n)}{\cos(a \cos(ib/n) + ic/n)}$$

and hence we have

$$\theta_i = a \cos\left(\frac{ib}{n}\right) + \frac{ic}{n}.$$

Note that the relative angles that determine the shape of the discrete serpenoid curve are given by

$$\phi_i := \theta_i - \theta_{i+1} = \alpha \sin\left(i \beta + \frac{\beta}{2}\right) + \gamma$$

where

$$\alpha := a \left| \sin\left(\frac{\beta}{2}\right) \right|, \quad \beta := \frac{b}{n}, \quad \gamma := -\frac{c}{n}.$$

Thus, the relative angle  $\phi_i$  changes in a sinusoidal manner along the “discrete arc length”  $i/n$  with the amplitude  $\alpha$  and the bias  $\gamma$ . Any two adjacent relative angles have the phase difference  $\beta$ .

## Serpentine Locomotion

The undulatory motion of a snake can be imitated by changing the relative angles of the snake robot in the following manner:

$$\phi_i = \alpha \sin(\omega t + (i-1)\beta) + \gamma, \quad (i = 1, \dots, n-1) \quad (19)$$

where  $\alpha$ ,  $\beta$ , and  $\gamma$  are the parameters that determine the shape of the serpenoid curve realized by the snake robot, and  $\omega$  specifies how fast the serpentine wave propagates along the body. Our hypothesis is that the serpentine gait is realized when the shape change as in (19) is coupled with the environment through the directional friction property.

In this section, we verify by numerical simulations that this hypothesis is indeed correct. Another objective here is to confirm that the following observation, made by Hirose [25] for snake robots with wheels, also applies to our no-wheel snake robot: The speed and the direction of the serpentine locomotion are mainly determined by  $\omega$  and  $\gamma$ , respectively.

We consider (16) and the first equation in (18) to describe the snake robot motion where the simple friction model  $D_f$  and  $D_\tau$  in (4) is used to define the matrices  $\mathcal{R}$ ,  $\mathcal{S}$ , and  $\mathcal{Q}$  as in (14). The robot parameters are specified as

$$n = 6, \quad m_i = 1 \text{ kg}, \quad l_i = 1 \text{ m}, \quad c_{t_i} = 0.1 \text{ Hz}, \quad c_{n_i} = 10 \text{ Hz}.$$

The input  $\dot{\phi}_i$  to (18) is generated to achieve the serpentine motion (19) asymptotically, and the locomotion of the snake robot is simulated with different parameter values for  $(\alpha, \beta, \gamma, \omega)$ . Typical motions are shown in Figs. 5 ( $\gamma = 0^\circ$ ) and 6 ( $\gamma = 10^\circ$ ) where the other parameters are fixed to

$$\alpha = 30^\circ, \quad \beta = 60^\circ, \quad \omega = 3 \text{ rad/s}.$$

The inertial  $(x, y)$  frame has been rotated after the simulation such that the average velocity of the center of gravity in the steady state (i.e., after the transients died out) is directed toward the positive  $x$ -axis. In each figure, the upper right picture shows the traces of the head (dashed line) and

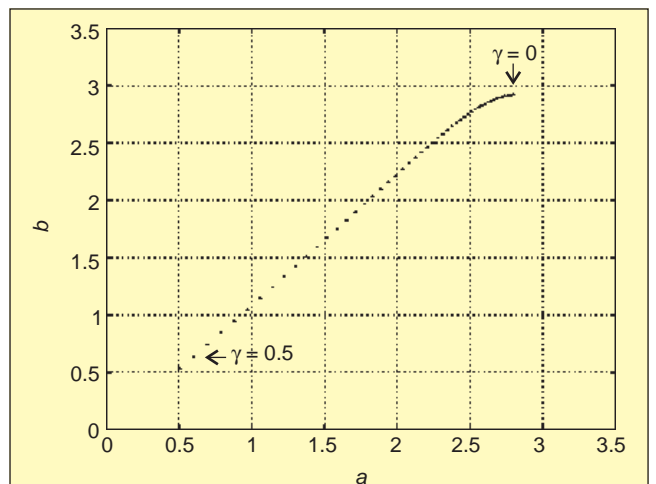


Figure 18. The parameters  $a$  and  $b$  for different values of  $\gamma$ .

## Some Integral Formulas

**Lemma 1:** Let scalars  $a, b$ , and  $c > 0$  be given. The following hold:

$$\frac{1}{2c} \int_{-c}^c \operatorname{sgn}(a + bs) ds = \operatorname{sat}(a, bc)$$

$$\frac{1}{c^2} \int_{-c}^c \operatorname{sgn}(a + bs) s ds = \operatorname{dzs}(a, bc)$$

where functions  $\operatorname{sat}(\cdot, \cdot)$  and  $\operatorname{dzs}(\cdot, \cdot)$  are defined by

$$\begin{aligned}\operatorname{sat}(x, y) &:= \begin{cases} 1 & (x > |y|) \\ x/y & (0 < |x| \leq |y|) \\ -1 & (x < -|y|) \\ 0 & (x = 0) \end{cases} \\ \operatorname{dzs}(x, y) &:= \begin{cases} 1 - (x/y)^2 & (y > |x|) \\ 0 & (|y| \leq |x|) \\ (x/y)^2 - 1 & (y < -|x|). \end{cases}\end{aligned}$$

**Proof:** It is straightforward to verify the result by calculating the integral for different cases. Hence the proof is omitted.

Note that  $\operatorname{sat}(\cdot, \cdot)$  and  $\operatorname{dzs}(\cdot, \cdot)$  are the saturation and the “dead zone saturation” functions that can be plotted as in Fig. 29. It is intuitively clear and easy to verify that both of these functions become the signum function in extreme cases

$$\operatorname{sat}(x, 0) = \operatorname{sgn}(x), \quad \operatorname{dzs}(0, y) = \operatorname{sgn}(y).$$

the center of gravity (solid line) and a snapshot of the snake robot at a certain time. We see that the snake robot moves in a straight line when  $\gamma = 0$  and moves along a circle when  $\gamma \neq 0$ . The lower left and lower right pictures show the time histories of the speed  $v$  and the angular speed  $\xi$  defined by

$$v := \dot{w}_x \cos \xi + \dot{w}_y \sin \xi, \quad \xi := \frac{1}{n} \sum_{i=1}^n \theta_i.$$

Note that  $\xi$  is the parameter that represents the direction of the whole snake robot and  $v$  is the speed of the center of gravity in the  $\xi$  direction. Both  $v$  and  $\xi$  oscillate with frequency  $\omega$  in the steady state, but their average values converge to certain constant values.

Next we fix  $\alpha$  and  $\beta$  as before and run the same simulations for different values of  $\omega$  and  $\gamma$ . The average values of the speed  $v$  and the angular speed  $\xi$ , denoted by  $\operatorname{ave}(v)$  and  $\operatorname{ave}(\xi)$ , are then obtained as functions of  $\omega$  and  $\gamma$  and are plotted in Figs. 7 and 8. The value of  $\operatorname{ave}(v)$  is the highest at the lower right corner of Fig. 7, whereas the value of  $\operatorname{ave}(\xi)$  is the

highest at the upper right corner of Fig. 8. We see that when  $\gamma$  is small,  $\operatorname{ave}(v)$  is determined by  $\omega$  and is insensitive to  $\gamma$ , whereas  $\operatorname{ave}(\xi)$  is determined by  $\gamma$  and is insensitive to  $\omega$ . Thus,  $\omega$  and  $\gamma$  are the dominant parameters for the speed and direction of the serpentine locomotion, respectively.

## Optimally Efficient Motion

In this section, we consider the serpentine motion along a straight line ( $\gamma = 0$ ) and show by simulations what choices of the parameters  $(\alpha, \beta, \omega)$  are most “efficient.” Let us first formally define the efficiency of the snake robot locomotion. Multiplying (13) by  $[\dot{\theta}' \dot{w}']$  from the left, we have the following power equation

$$P_k + P_l = P_i$$

with

$$\begin{aligned}P_k &:= \frac{d}{dt} \left( \frac{1}{2} \dot{\theta}' \mathcal{J} \dot{\theta} + \frac{m}{2} \dot{w}' \dot{w} \right) \text{(kinetic power)} \\ P_l &:= \begin{bmatrix} \dot{\theta}' \\ \dot{w}' \end{bmatrix} \begin{bmatrix} \mathcal{R} & \mathcal{S} \\ \mathcal{S}' & \mathcal{Q} \end{bmatrix} \begin{bmatrix} \dot{\theta} \\ \dot{w} \end{bmatrix} \text{(power loss)} \\ P_i &:= \dot{\phi}' u \text{(input power)}\end{aligned}$$

where we noted from (15) that

$$\begin{aligned}\frac{d}{dt} \left( \frac{1}{2} \dot{\theta}' \mathcal{J} \dot{\theta} \right) &= \dot{\theta}' \mathcal{J} \ddot{\theta} + \frac{1}{2} \dot{\theta}' \mathcal{J}' \dot{\theta} \\ &= \dot{\theta}' \mathcal{J} \ddot{\theta} + \frac{1}{2} \dot{\theta}' (\mathcal{C} \dot{\theta} + \dot{\theta} \mathcal{C}') \dot{\theta} \\ &= \dot{\theta}' \mathcal{J} \ddot{\theta} + \dot{\theta}' \mathcal{C} \dot{\theta}^2.\end{aligned}$$

From the power equation, we see that part of the input power  $P_i$  from the joint actuator is converted to the kinetic power  $P_k$  and the rest is lost as  $P_l$  due to the friction. In fact, the power loss is essential for snake locomotion, since it is the friction force that generates the forward acceleration. In the steady state, the average kinetic energy is constant, and hence the average kinetic power  $\operatorname{ave}(P_k)$  is zero. In this case, on average, all the input power  $P_i$  supplied by the joint actuators is consumed as the power loss  $P_l$  due to the friction.

The objective of this section is to find the optimally efficient motion within the framework of serpentine locomotion. More precisely, we investigate for what choices of the parameters  $(\alpha, \beta, \omega)$  the average power loss,  $\operatorname{ave}(P_l)$ , is minimal while keeping a prescribed average speed,  $\operatorname{ave}(v)$ .

Gridding the parameter space as  $\alpha = 3, 6, 9, \dots, 90^\circ$ ,  $\beta = 6, 12, 18, \dots, 180^\circ$ , and  $\omega = 0.5, 1, 1.5, \dots, 5$  rad/s, the quantities  $\operatorname{ave}(P_l)$  and  $\operatorname{ave}(v)$  are computed via simulations for each parameter triplet  $(\alpha, \beta, \omega)$  and are plotted in Fig. 9(a). The figure clearly shows the Pareto optimal curve corresponding to the minimum power with fixed values of the speed. Extracting the points on the curve, one can find the optimal relationship between the average forward speed  $\operatorname{ave}(v)$  and

the frequency  $\omega$  [Fig. 9(b)]. As seen in the figure,  $\text{ave}(v)$  and  $\omega$  are roughly proportional to each other. The Pareto optimal points are plotted in the  $(\alpha, \beta, \omega)$  space together with their projections onto the three planes in Fig. 10. Note that the Pareto optimal phase-shift  $\beta$  is independent of the other variables and is  $\beta \approx 60^\circ$ .

Next we run the same simulations with different numbers of links  $n$  to see how the optimally efficient parameters depend upon  $n$ . For each value of  $n = 3, \dots, 10$ , figures similar to Fig. 10 can be drawn, and the qualitative properties of the optimal parameters are found not to depend upon  $n$ . The mean value (over  $1 \leq \omega \leq 4.5$ ) of the optimal  $\alpha$  is found to be insensitive to  $n$ , whereas that of  $\beta$  significantly changes with  $n$ , as shown in Fig. 11. It seems that the Pareto optimal value of  $\beta$  is essentially determined by the number of links only and is roughly equal to  $2\pi/n$  (the solid curve in Fig. 11). This means that the snake robot forms just one period of the serpenoid curve when the power efficiency is optimized.

Finally, we run the same simulations with different values of the friction coefficient  $c_t$ . The relationship between the mean value of the optimal  $\alpha$  and the ratio  $c_t/c_n$  is shown in Fig. 12. We see that  $\alpha$  is an increasing function of  $c_t/c_n$ . Thus, the snake robot should undulate with larger amplitude when the ratio  $c_t/c_n$  is larger (i.e., when the snake robot is more likely to slip in the normal direction).

In summary, we have found the following properties of the Pareto optimal parameters:

- $\omega$  is a linear function of the forward speed.
- $\alpha$  is an increasing function of the ratio  $c_t/c_n$  of the friction coefficients.
- $\beta$  is a decreasing function of  $n$ ; roughly,  $\beta = 2\pi/n$ .

These observations are useful for (heuristically) determining the optimal control law for the snake robot.

## Synthesis of Snakelike Locomotion

### Control Architecture

Recall from the analysis in the previous section that the parameters  $\omega$  and  $\gamma$  in the serpentine motion determine the speed and direction of the snake robot, respectively. On the other hand, we found that the values of  $\alpha$  and  $\beta$  that give optimal efficiency are determined by the friction coefficients and the number of links, respectively. Hence we fix  $\alpha$  and  $\beta$  and use  $\omega$  and  $\gamma$  to control the speed and direction of the snake robot. In the simulations shown below, we consider the five-link snake robot ( $n = 5$ ) with  $m_i = 1 \text{ kg}$  and  $l_i = 1 \text{ m}$ , and we fix  $\alpha$  and  $\beta$  to the following values:

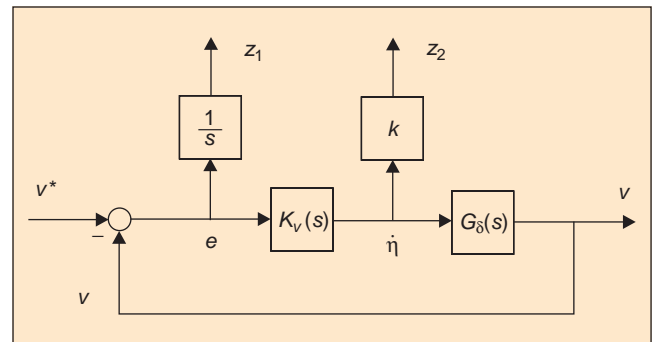
$$\alpha = \frac{\pi}{2}, \quad \beta = \frac{2\pi}{n}.$$

Fig. 13 shows the block diagram of the basic control system. The block labeled “Snake Robot” is given by (13). The controller mainly consists of inner/outer loops. The outer-loop controllers  $C_v(s)$  and  $C_\xi(s)$  are, respectively, for speed and direction controls and generate the command motion variable  $\phi^*$  through the time-varying transformation (represented by  $T$ )

$$\phi_i^* := \alpha \sin(\omega t + (i-1)\beta) + \gamma$$

to achieve the desired motion  $v^*$  and  $\xi^*$ . The inner-loop controller  $C_\phi(s)$  generates the torque  $u$  so that the actual motion  $\phi$  follows the command signal  $\phi^*$ .

In the first-round design, we tried proportional-integral-derivative (PID) controllers for  $C_v(s)$ ,  $C_\xi(s)$ , and  $C_\phi(s)$  and found that the design was not successful. In particular,



**Figure 19.** Speed control system.

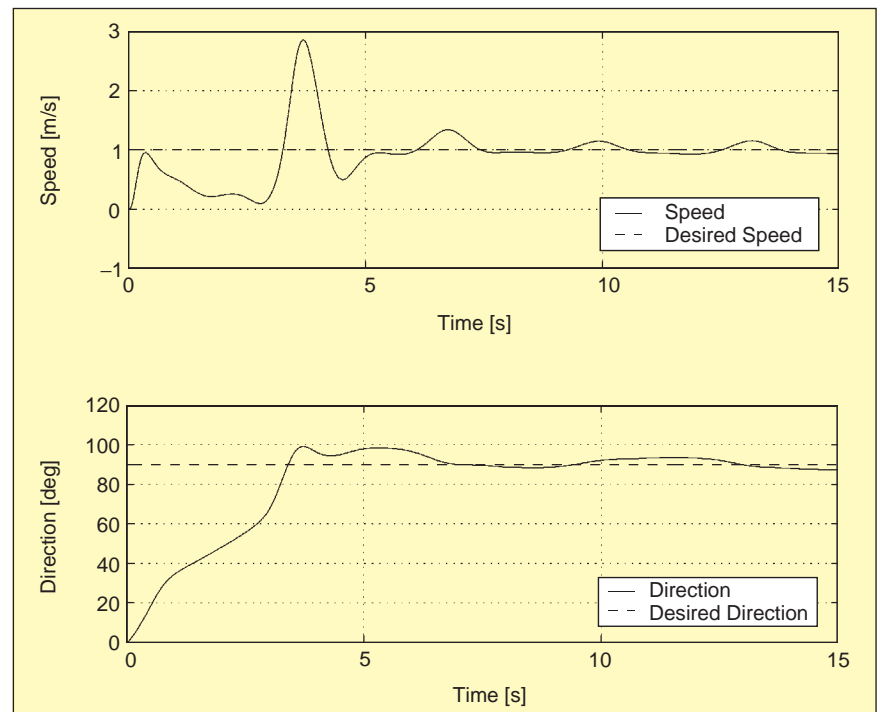


**Figure 20.** Simulation result (simple friction model).

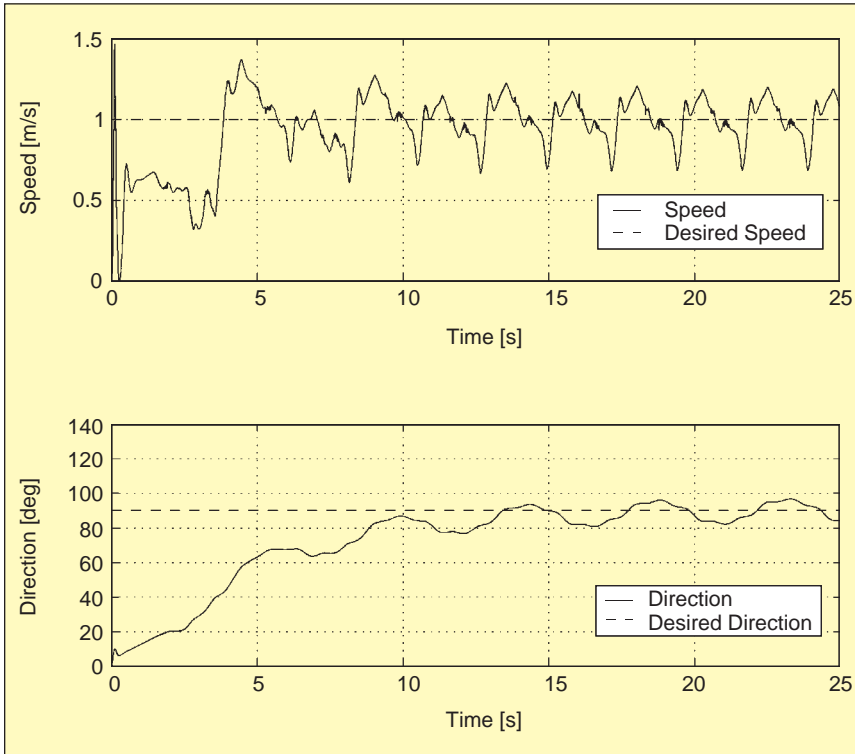


**Figure 21.** Simulation result (Coulomb friction model).

we had difficulty tuning the PID parameters to yield satisfactory motion control performance, especially for speed control. Hence we decided to use PID controllers for  $C_\xi(s)$  and  $C_\phi(s)$  and to design  $C_v(s)$  in a more sophisticated manner. We explain the procedure for designing  $C_v(s)$  in the next section.

### Speed Control System

In this section, we develop a speed control system  $C_v(s)$  within the control architecture introduced in the previous section. In the sequel, we use the simple friction model of

the snake robot with  $c_{t_i} = 0.1$  Hz and  $c_{n_i} = 10$  Hz for control design. The more realistic Coulomb friction model will be used for simulations to validate our result after the control design.

To examine how the variable  $\omega$  affects the speed  $v$ , we have changed  $\omega(t)$  in a sinusoidal manner and observed  $v(t)$  by simulation. As a result, we found that  $v(t)$  is also a sinusoidlike signal, but with an increasing amplitude diverging to infinity. Thus, the mapping from  $\omega$  to  $v$  is not bounded-input, bounded-output (BIBO) stable, and this fact motivated us to consider a new control input that gives a BIBO stable mapping and hence would be more suitable for speed control.

Here we introduce the following variable  $\dot{\eta}$  as a new control input

$$\dot{\eta} := \frac{d\eta}{dt} = \dot{\omega}t + \omega, \quad \eta := \omega t.$$

Note that  $\dot{\eta}$  is the “effective frequency” of the sinusoidal signal  $\sin(\omega t)$  with time-varying frequency  $\omega$ . If  $\dot{\eta}(t)$  is sinusoidal, so is the signal  $\eta = \omega t$ . Hence  $\omega(t)$  approaches zero as the time goes to infinity, even though  $\dot{\eta}(t)$  is a sinusoidal signal with a fixed amplitude. Thus, we expect that when  $\dot{\eta}$  is sinusoidal, the resulting speed  $v$  would not diverge and the mapping from  $\dot{\eta}$  to  $v$  would be BIBO stable. We found by simulation that this is indeed the case.

We have run simulations for sinusoidal inputs  $\dot{\eta}$  using the simple friction model. In particular,  $\dot{\eta}$  is chosen as

$$\dot{\eta} = \chi \sin(\lambda t)$$

for fixed values of  $\lambda$  and  $\chi$ . The value of  $\chi$  is set to 1 rad/s. We have tried other values as well and found that the results given below are insensitive to  $\chi$ . The motion variable  $\dot{\phi}_i$  is calculated by

$$\dot{\phi}_i(t) = \alpha \cos(\eta(t)) + (i-1)\beta \dot{\eta}(t)$$

and is applied as the input to the snake robot model (18). Note that the initial value  $\eta(0)$  is equal to zero by definition.

Typical speed responses are plotted in Fig. 14 for the case  $\lambda = 0.01$  and in Fig. 15 for the case  $\lambda = 5$ . From Fig. 14 we see that the output signal  $v$  contains high-frequency harmonics, but the largely dominant part is the sinusoid with the same frequency as the input. When the input frequency is higher (see Fig. 15), a similar comment applies as well, with a notable difference being that the phase lag and the amplitude attenuation of the output  $v$  are more apparent. This means

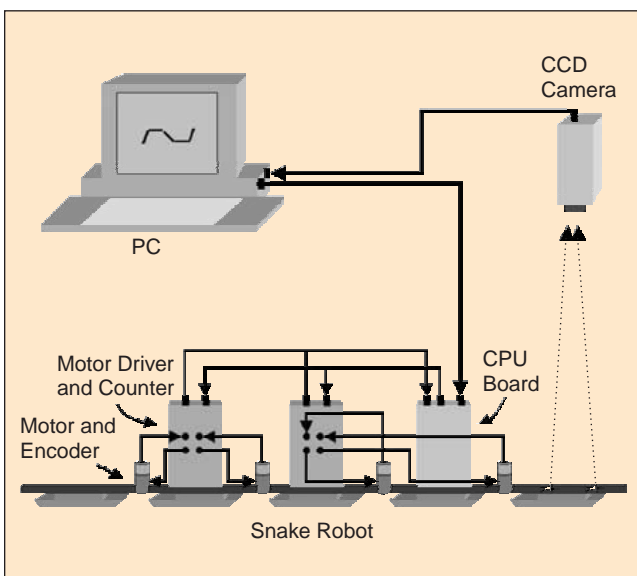


**Figure 22.** System configuration.

that the mapping from  $\dot{\eta}$  to  $v$  is almost linear! Thus, choosing the effective frequency  $\dot{\eta}$  as the input, the highly nonlinear robot dynamics can be quasi-linearized.

Repeating the simulation for different values of  $\lambda$ , we obtain a “frequency response” of the snake robot from the input  $\dot{\eta}$  to the output  $v$ , where we ignore the higher frequency harmonics of the output signal. The gain and phase plots thus obtained are shown by the solid curves in Fig. 16. From the figure we see that the mapping from  $\dot{\eta}$  to  $v$  may be approximated by a first-order transfer function given by

$$G(s) = \frac{2.8517}{s + 2.8286}$$

whose frequency response is plotted by the dashed lines in Fig. 16. Thus, introducing a new control input  $\dot{\eta}$ , we may approximate the dynamics of the snake robot by a simple first-order transfer function. Clearly, such approximation should be useful for speed control design.

The above approximated model is valid only for the case  $\gamma = 0$  in the serpentine motion

$$\phi_i(t) = \alpha \sin(\omega t + (i-1)\beta) + \gamma.$$

Recall that  $\gamma$  is used to control the direction of the snake locomotion, and we need to consider the case where  $\gamma$  is non-zero as well to allow for the directional control. Here we consider values of  $\gamma$  such that  $|\gamma| \leq 0.5$ .

Since the locomotion of the snake robot is “symmetric” in  $\gamma$ , we consider the interval  $0 \leq \gamma \leq 0.5$ . For each value of  $\gamma$  within the interval, we obtained the frequency response from  $\dot{\eta}$  to  $v$  as described above. The responses are approximated by first-order transfer functions and plotted in Fig. 17. The transfer function for each  $\gamma$  is given by

$$G(s) = \frac{b}{s + a},$$

where the parameters  $a$  and  $b$  vary with  $\gamma$ , as shown in Fig. 18. We see that the values of  $a$  and  $b$  are approximately the same for each fixed  $\gamma$  and vary in the interval  $0.5 \leq a \approx b \leq 3$ . Thus, we have the following linear system model with an uncertain parameter  $\delta$ :

$$G_\delta(s) = \frac{a}{s + a}, \quad a := a_0 + \delta a_1, \quad |\delta| \leq 1,$$

where  $a_0 := 1.75$  and  $a_1 := 1.25$ . This model is suitable for robust control design.

We design a controller such that the speed  $v$  of the snake robot closely follows a given command signal  $v^*$ . In particular, we consider the block diagram in Fig. 19 and design  $K_v(s)$  that minimizes an upper bound on the worst-case  $L_2$  gain (see, e.g., [34], [35]) from  $v^*$  to  $z := [z_1 \ z_2]'$ , where the worst case is taken over all possible time-varying paramet-

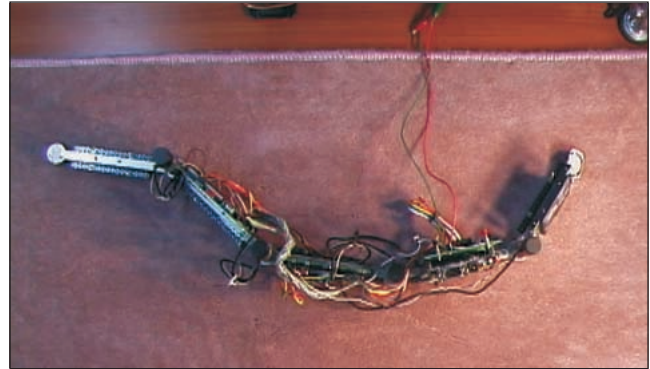


**Figure 23.** Top view of the snake robot.



**Figure 24.** The “belly” of the snake robot.

ric uncertainties  $\delta(t) \in [-1, 1]$ . The parameter  $k$  is the weight on the control signal  $\dot{\eta}$ , to be specified later.

The generalized plant for this control system is given by

$$\begin{bmatrix} \dot{v} \\ \dot{x} \\ z_0 \\ z_1 \\ z_2 \\ y \end{bmatrix} = \begin{bmatrix} -a_0 & 0 & a_1 & 0 & a_0 \\ -1 & 0 & 0 & 1 & 0 \\ -1 & 0 & 0 & 0 & 1 \\ 0 & 1 & 0 & 0 & 0 \\ 0 & 0 & 0 & 0 & k \\ -1 & 0 & 0 & 1 & 0 \end{bmatrix} \begin{bmatrix} v \\ x \\ w \\ v^* \\ \dot{v} \\ \dot{\eta} \end{bmatrix}, \quad w = \delta z_0.$$

Approximating the worst-case  $L_2$  gain by the scaled  $H_\infty$  norm [36], [37], we obtain a controller that minimizes the scaled  $H_\infty$  norm as follows:

$$K_v(s) = 0.8327 + \frac{0.9021}{s}$$

where the design parameter is chosen to be  $k = 1$  by trial and error. Note that the controller turned out to have the proportional-integral structure.

## Simulation Results

We now have a total control system for the snake robot in which the mapping from  $(v^* - v)$  and  $(\xi^* - \xi)$  to  $\dot{\phi}^*$  in Fig. 13 is replaced by

$$\begin{aligned}\eta &= \frac{1}{s} K_v(s)(v^* - v), \quad \gamma(s) = C_\xi(s)(\xi^* - \xi), \\ \phi^* &= \alpha \sin(\eta + (i-1)\beta) + \gamma.\end{aligned}$$

The controllers  $C_\xi(s)$  and  $C_\phi(s)$  are chosen to have the PID structure and their parameters tuned by trial and error. The controller  $K_v(s)$  is the one designed in the previous section via a scaled  $H_\infty$  synthesis method.

In our simulation, the parameters of the snake robot are chosen as

$$l_i = 1 \text{ m}, \quad m_i = 1 \text{ kg}, \quad (i = 1, \dots, n).$$

The command velocity signals

$$v^*(t) := 1 \text{ m/s}, \quad \xi^*(t) := \frac{\pi}{2} \text{ rad}$$

are applied when the snake robot is initially straight ( $\theta_i(0) = 0$ ) and at rest ( $\dot{\theta}_i(0) = 0, \dot{w}(0) = 0$ ).

First, we run a simulation for the simple friction model with the following parameters:

$$\begin{aligned}c_{t_i} &= 0.1, \quad c_{n_i} = 10, \quad (i = 1, \dots, n) \\ C_\xi(s) &= -1, \quad C_\phi(s) = \left(100 + \frac{10}{s} + 10s\right)I.\end{aligned}$$

The result is shown in Fig. 20, where the dashed lines in the speed  $v$  and direction  $\xi$  plots indicate the commanded signals and the solid lines are the actual responses of the snake robot. The transient response of the speed may not seem adequate; however, it is a result of our tuning the controller  $C_\xi(s)$  such that the snake robot starts moving with both the desired speed and the desired direction as soon as possible. When controlling a snake robot, it does not make sense to

have it move at the right speed in the wrong direction. Thus, in our view, the responses in Fig. 20 are satisfactory.

Next we run a simulation for the Coulomb friction model with the following parameters:

$$\begin{aligned}\mu_{t_i} &= 0.1, \quad \mu_{n_i} = 10, \quad (i = 1, \dots, n) \\ C_\xi(s) &= -0.35, \quad C_\phi(s) = \left(500 + \frac{30}{s} + 10s\right)I.\end{aligned}$$

The result is shown in Fig. 21. We see that the speed and direction responses are more oscillatory than the case of the simple friction model, but the effect of these oscillations on the actual trajectory is not substantial.

## Experimental Validation

In this section, we validate our control design strategy through a laboratory experiment.

### System Configuration

The experimental testbed mainly consists of five components—a snake robot, motor drivers, a CPU board, a charge-coupled device (CCD) camera, and a PC (see Fig. 22).

The snake robot is simply a connection of five rigid links with four joints with total weight of 1.8 kg (Fig. 23). Each link is made of aluminum of length 0.15 m and has edges at the bottom that generate larger friction forces in the normal direction than in the tangential direction (Fig. 24).

Mounted on each joint is a 1.7 W dc motor (RH-5A Harmonic Drive; Linx) with an embedded encoder (28,000 pulses per revolution). The motor drivers and the CPU board are mounted on the snake robot. Two voltages (5 V for logic circuits on the motor drivers and the CPU board and 12 V for driving the motor) are supplied through cables.

The CCD camera (CV-10BX; JAI) collects 30 images per second and is used to detect the positions of two marked points on the first link of the snake robot.

The PC receives the image data from the camera every 33 ms and computes the coordinates  $(x_1, y_1)$  of the middle point and the absolute angle  $\theta_1$  of the first link. This image processing takes about 60 ms, and hence approximately one out of two image data points from the CCD camera is discarded. Information on the position and orientation of the first link is sent from the PC to the CPU board through an RS-232C serial cable.

The CPU board calculates the command torque  $r$  (more precisely, a quantity to be used as the duty ratio  $r$  of the PWM signal, as explained below) using the velocity command signal  $(v^*, \xi^*)$ , the position/orientation information from the PC, and the relative angle in-

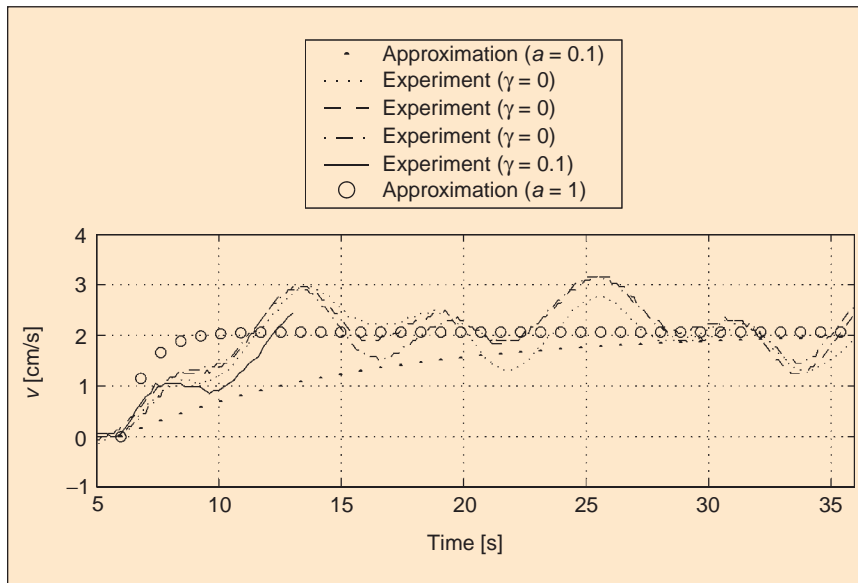


**Figure 25.** Step responses.

formation from the counter, all based on the control rule previously discussed, where  $u$  is replaced by  $r$ . The sampling rate of the CPU board is 10 ms.

The motor drivers receive the torque command  $r$  from the CPU board and then generate PWM voltage signals with the duty ratio  $r_i$  for the motor on the  $i$ th joint, where  $r_i$  ( $i = 1, \dots, n-1$ ) is the  $i$ th entry of the vector  $r$ .

## Modeling and Control Design

The first step in our control design is the modeling of the snake robot. Instead of taking the frequency responses from  $\dot{\eta}$  to  $v$ , as in the previous section, we choose to model the system by step responses for simplicity. Another difference from the simulation case is that the minor feedback loop for the shape control is implemented first as follows:

$$C_\phi(s) = 20 + \frac{7}{s} + 2s$$

and then step responses are taken for the snake robot with the minor feedback loop. Fig. 25 shows the responses  $v$  when the step inputs of magnitude  $\pi/6$  rad are applied at time  $t = 6$  s to  $\dot{\eta}$  with different values of  $\gamma$ . We have also observed step responses with different input magnitudes and found, as in the simulation study, that the responses normalized by the input magnitudes are insensitive to the input magnitudes. The three responses for  $\gamma = 0$  are obtained through three different experiments. The responses are found to be oscillatory, but we go on to obtain a crude approximation of the system from  $\dot{\eta}$  rad to  $v$  m/s as follows:

$$G_\delta(s) = 0.0382 \times \frac{a}{s+a}, \quad a := a_0 + \delta a_1, \quad |\delta| \leq 1,$$

where  $a_0 := 0.55$  and  $a_1 := 0.45$ . The step responses of  $G_\delta(s)$  for  $\delta = \pm 1$  are also shown in Fig. 25.

Based on this linear uncertain system model, we designed a controller  $K_v(s)$  rad/m as described in the previous section with the design parameter  $k = 0.1$  as follows:

$$K_v(s) = 25.53 + \frac{6.642}{s}.$$

The parameters of the PID controller  $C_\xi(s)$  are tuned through actual experiments, and a suitable controller is found to be a simple constant gain

$$C_\xi(s) = -0.1.$$

The control system thus obtained is discretized via the Tustin transformation (e.g., [38]) with the sampling rate of 10 ms and implemented on the CPU board.

## Experimental Results

An experiment is conducted under the following conditions. The step velocity commands

$$\begin{aligned} v^*(t) &:= 0.013160 \text{ m/s} \\ \xi^*(t) &:= 0 \text{ rad} \end{aligned}$$

are applied when the snake robot is at rest and its body is straight at an angle of about  $25^\circ$  from the desired direction of locomotion.

Fig. 26 shows the motion pictures of the snake robot where the white and black arrows, respectively, indicate the initial and desired directions of the snake motion. Fig. 27 shows the time histories of the speed  $v$  of the center of gravity and the direction  $\xi$  of the whole body. We see that the speed  $v$  satisfactorily tracks the desired speed. The direction parameter  $\xi$  is oscillatory, but its average is approximately zero, meaning that the snake robot is moving toward the desired direction on average. To justify this claim, the motion of the snake robot is shown on the  $x$ - $y$  plane using the experimental data (Fig. 28). The snake robot moves from right to left in the figure. We see that the direction of the snake robot is not aligned with the desired direction at the beginning, but the robot soon begins moving in the desired direction.

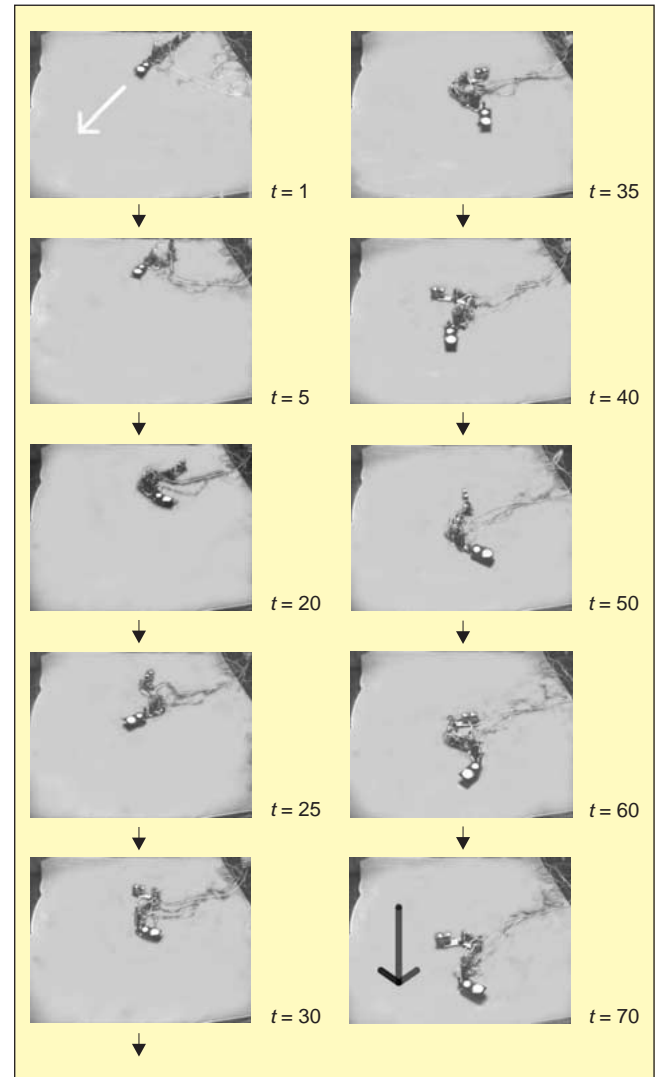


**Figure 26.** Locomotion of the snake robot.

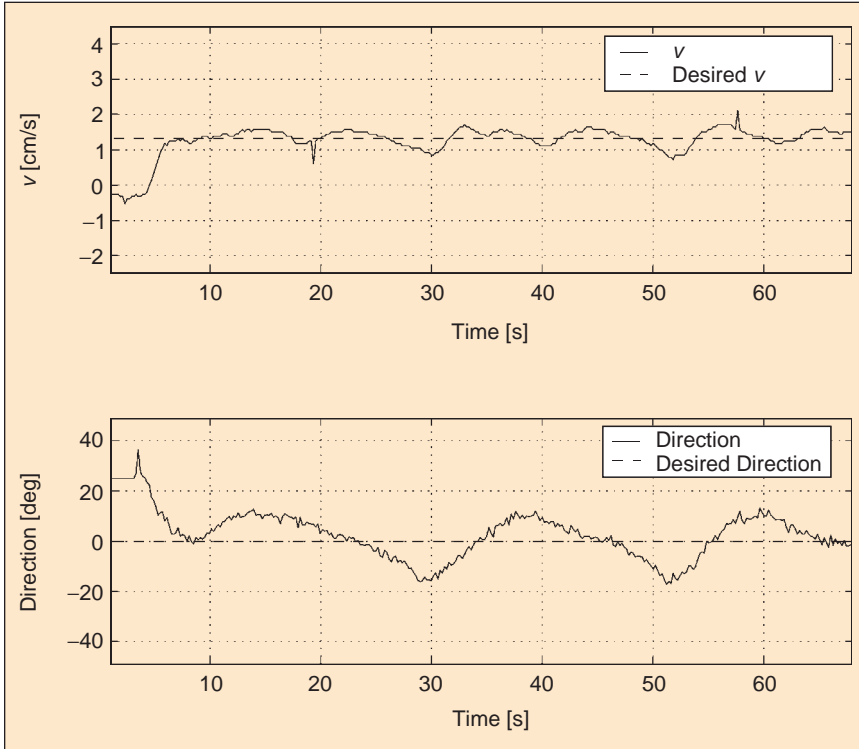


**Figure 27.** Speed and direction of the snake robot.

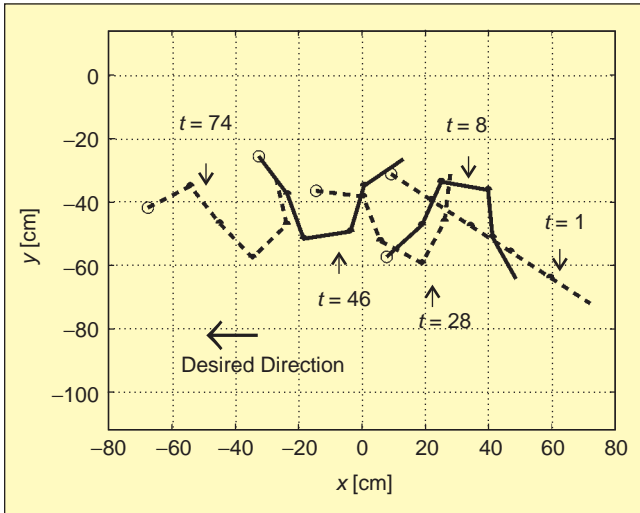


**Figure 28.** Snake motion from the experimental data.

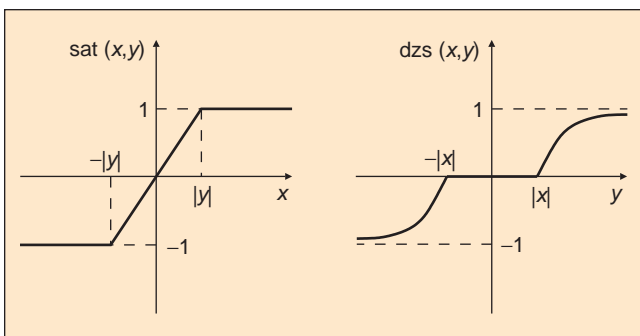


**Figure 29.** Functions  $\text{sat}(\cdot)$  and  $\text{dzs}(\cdot)$ .

In summary, we conclude that our control strategy yielded a reasonable velocity control system for the locomotion of the snake robot.

## Conclusion

We have described a snake robot without wheels and developed its model based on the directional friction coefficients. After the model transformation that decouples the inertial locomotion from the internal shape motion, an optimally efficient serpentine locomotion is investigated. Based on the analysis results, a velocity control scheme is proposed using a quasilinearizing input transformation, and its validity is demonstrated via a laboratory experiment with a five-link serpentine robot.

The results reported in this article focused on the planar serpentine gait that is suited for locomotion in an environment where friction with directional preference can be realized. A mathematical framework is estab-

lished for modeling, analysis, and synthesis of the serpentine gait, but the tremendous adaptability of the snakelike mechanism to rugged environments has not yet been fully exploited. Studies of other gaits remain to be done to make a snake robot capable of, for example, adapting to isotropic friction environments and/or performing three-dimensional motion.

## Acknowledgments

We gratefully acknowledge helpful discussions with B.D.O. Anderson, S. Hirose, T. Mita, P. Prautsch, H. Yamauchi, and R. Nakashima. This research is supported by The Grant-in-Aid for Center-of-Excellence Research Project of Super Mechano-Systems by The Ministry of Education, Science, Sport and Culture in Japan.

## References

- [1] M. Raibert, *Legged Robots that Balance*. Cambridge, MA: MIT Press, 1986.
- [2] S. Song and K. Waldron, *Machines that Walk: The Adaptive Suspension Vehicle*. Cambridge, MA: MIT Press, 1989.
- [3] D.J. Manko, *A General Model of Legged Locomotion on Natural Terrain*. Norwell, MA: Kluwer, 1992.
- [4] M. Vukobratovic, B. Borovac, D. Surla, and D. Stokic, *Biped Locomotion: Dynamics, Stability, Control and Application*. New York: Springer-Verlag, 1990.
- [5] P. Spanos, R. Berka, and P. Tratskas, "Multisegment large space robot: Concept and design," *J. Aerosp. Eng.*, vol. 13, no. 4, pp. 123-132, 2000.
- [6] D. Reznik and V. Lumelsky, "Sensor-based motion planning in 3 dimensions for a highly redundant snake robot," *Adv. Robot.*, vol. 9, no. 3, pp. 255-280, 1995.

- [7] Y. Shan and Y. Koren, "Design and motion planning of a mechanical snake," *IEEE Trans. Syst. Man Cybern.*, vol. 23, pp. 1091-1100, 1993.
- [8] Z. Bayraktaroglu, F. Butel, P. Blazevic, and V. Pasqui, "Geometrical approach to the trajectory planning of a snake-like mechanism," in *Proc. IEEE Int. Conf. Intel. Robots Sys.*, Kyongju, Korea, 1999, pp. 1322-1327.
- [9] B. Klaassen and K. Paap, "GMD-SNAKE2: A snake-like robot driven by wheels and a method for motion control," in *Proc. IEEE Int. Conf. Robot. Auto.*, Detroit, MI, 1999, pp. 3014-3019.
- [10] S. Ma, "Analysis of snake movement forms for realization of snake-like robot," in *Proc. IEEE Int. Conf. Robot. Auto.*, Detroit, MI, 1999, pp. 3007-3013.
- [11] K. Dowling, "Limbless locomotion: Learning to crawl," in *Proc. IEEE Int. Conf. Robot. Auto.*, Detroit, MI, 1999, pp. 3001-3006.
- [12] G. Poi, C. Scarabeo, and B. Allotta, "Traveling wave locomotion hyper-redundant mobile robot," in *Proc. IEEE Int. Conf. Robotics & Automation*, Leuven, Belgium, 1998, pp. 418-423.
- [13] L. Jammes, Y. Kyodo, M. Hiraki, and S. Ozono, "Design concept and undulatory motion mode of a modular snake-like robot," in *Proc. IEEE Int. Conf. Intel. Robots Sys.*, Grenoble, France, 1997, pp. 1794-1799.
- [14] M. Nilsson, "Snake robot free climbing," *IEEE Control Syst. Mag.*, vol. 18, pp. 21-26, 1998.
- [15] R. Worst and R. Linnemann, "Construction and operation of a snake-like robot," in *Proc. IEEE Int. Joint Symp. Intelligent Systems*, Gaithersburg, MD, 1996, pp. 164-169.
- [16] J. Gray and H. Lissmann, "The kinetics of locomotion of the grass-snake," *J. Exp. Biol.*, vol. 26, no. 4, pp. 354-367, 1950.
- [17] H. Lissmann, "Rectilinear locomotion in a snake (*Boa occidentalis*)," *J. Exp. Biol.*, vol. 26, pp. 368-379, 1950.
- [18] B.C. Jayne, "Kinematics of terrestrial snake locomotion," *Copeia*, vol. 4, pp. 915-927, 1986.
- [19] B.C. Jayne, "Muscular mechanisms of snake locomotion: An electromyographic study of the sidewinding and concertina modes of *Crotalus cerastes*, *Nerodia fasciata* and *Elaphe obsoleta*," *J. Exp. Biol.*, vol. 140, pp. 1-33, 1988.
- [20] B.C. Jayne and J.D. Davis, "Kinematics and performance capacity for the concertina locomotion of a snake (*Coluber constrictor*)," *J. Exp. Biol.*, vol. 156, pp. 539-556, 1991.
- [21] S. Secor, B. Jayne, and A. Bennett, "Locomotor performance and energetic cost of sidewinding by the snake *Crotalus cerastes*," *J. Exp. Biol.*, vol. 163, pp. 1-14, 1992.
- [22] S. Bennet, T. McConnell, and S. Trubatch, "Quantitative analysis of the speed of snakes as a function of peg spacing," *J. Exp. Biol.*, pp. 161-165, 1974.
- [23] Y. Umetani and S. Hirose, "Biomechanical study of serpentine locomotion," in *Proc. 1st RoManSy Symp.*, Udine, Italy, 1974, pp. 171-184.
- [24] S. Hirose and Y. Umetani, "Kinematic control of active cord mechanism with tactile sensors," in *Proc. 2nd RoManSy Symp.*, Warsaw, Poland, 1976, pp. 249-260.
- [25] S. Hirose, *Biologically Inspired Robots: Snake-Like Locomotors and Manipulators*. New York: Oxford Univ. Press, 1993.
- [26] S. Hirose and A. Morishima, "Design and control of a mobile robot with an articulated body," *Int. J. Robot. Res.*, vol. 9, no. 2, pp. 99-114, 1990.
- [27] J. Burdick, J. Radford, and G. Chirikjian, "A 'sidewinding' locomotion gait for hyper-redundant robots," *Adv. Robot.*, vol. 9, no. 3, pp. 195-216, 1995.
- [28] G. Chirikjian and J. Burdick, "The kinematics of hyper-redundant robot locomotion," *IEEE Trans. Robot. Automat.*, vol. 11, pp. 781-793, 1995.
- [29] J. Ostrowski and J. Burdick, "The geometric mechanics of undulatory robotic locomotion," *Int. J. Robot. Res.*, vol. 17, no. 7, pp. 683-701, 1998.
- [30] P. Prautsch, T. Mita, and T. Iwasaki, "Analysis and control of a gait of snake robot," *Trans. IEE J. Ind. Appl. Soc.*, vol. 120-D, pp. 372-381, 2000.
- [31] H. Date, Y. Hoshi, and M. Sampei, "Locomotion control of a snake-like robot based on dynamic manipulability," in *Proc. IEEE Int. Conf. Intell. Robots and Syst.*, Takamatsu, Japan, 2000, pp. 2236-2241.
- [32] K. Kyriakopoulos, G. Migadis, and K. Sarrigeorgidis, "The NTUA snake: Design, planar kinematics, and motion planning," *J. Robot. Syst.*, vol. 16, no. 1, pp. 37-72, 1999.
- [33] R.M. Murray, Z. Li, and A.S. Sastry, *A Mathematical Introduction to Robotic Manipulation*. Boca Raton, FL: CRC, 1993.
- [34] R.E. Skelton, T. Iwasaki, and K.M. Grigoriadis, *A Unified Algebraic Approach to Linear Control Design*. London, U.K.: Taylor & Francis, 1997.
- [35] K. Zhou, J. Doyle, and K. Glover, *Robust and Optimal Control*. Upper Saddle River, NJ: Prentice-Hall, 1996.
- [36] J.C. Doyle, A. Packard, and K. Zhou, "Review of LFTs, LMIs, and  $\mu$ ," in *Proc. IEEE Conf. Decision Contr.*, Brighton, U.K., 1991, pp. 1227-1232.
- [37] A. Packard, K. Zhou, P. Pandey, and G. Becker, "A collection of robust control problems leading to LMIs," in *Proc. IEEE Conf. Decision Contr.*, Brighton, U.K., 1991, pp. 1245-1250.
- [38] G.F. Franklin, J.D. Powell, and M.L. Workman, *Digital Control of Dynamic Systems*. Reading, MA: Addison-Wesley, 1990.

**Masashi Saito** received the B.E. and M.E. degrees in control systems engineering from Tokyo Institute of Technology in 1998 and 2000, respectively. Currently, he is an engineer in the 1st Electronic Device Design Department, the Automotive Products Division, at Hitachi, Ltd., working on research and development of control systems for automotive engine, electric throttle control modules, and electric shift actuator modules.

**Masakazu Fukaya** received the B.E. and M.E. degrees in control systems engineering from Tokyo Institute of Technology in 1999 and 2001, respectively. Currently, he is working at Fujitsu company as an engineer. His research interests include nonholonomic systems, multirate digital control, and variable constraint control.

**Tetsuya Iwasaki** received the B.E. and M.E. degrees in electrical and electronic engineering from Tokyo Institute of Technology in 1987 and 1990, respectively, and the Ph.D. degree from the School of Aeronautics and Astronautics, Purdue University, in 1993. After holding a faculty position for five years at Tokyo Institute of Technology, he moved to the University of Virginia in May 2000, where he is currently an Assistant Professor. His research interests include control systems in general, and modeling/control of biological sensing, locomotion, and oscillation. He is on the editorial boards of the *IEEE Transactions on Automatic Control* and *Systems and Control Letters*.